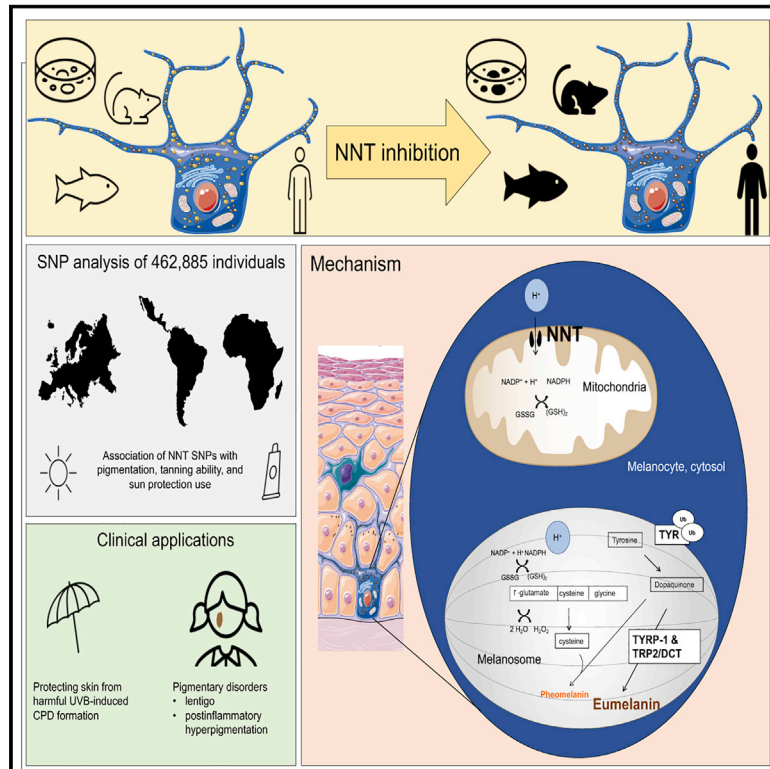


NNT mediates redox-dependent pigmentation via a UVB- and MITF-independent mechanism

Graphical abstract



Authors

Jennifer Allouche, Inbal Rachmin, Kaustubh Adhikari, ..., Andrés Ruiz-Linares, David E. Fisher, Elisabeth Roeder

Correspondence

dfisher3@mgh.harvard.edu (D.E.F.), eroeder@cbr2.mgh.harvard.edu (E.R.)

In brief

Nicotinamide nucleotide transhydrogenase (NNT) is a mitochondrial redox-regulating enzyme that mediates pigmentation via a UVB- and MITF-independent mechanism.

Highlights

- Identification of a redox-dependent skin pigmentation mechanism
- Modification of NNT affects ubiquitin-proteasome-mediated tyrosinase degradation
- Alteration of NNT levels affects skin pigmentation through melanosome maturation
- Human NNT SNPs are associated with skin pigmentation, tanning, and use of sun protection



Article

NNT mediates redox-dependent pigmentation via a UVB- and MITF-independent mechanism

Jennifer Allouche,^{1,38} Inbal Rachmin,^{1,38} Kaustubh Adhikari,^{2,3,39} Luba M. Pardo,^{4,39} Ju Hee Lee,⁵ Alicia M. McConnell,⁶ Shinichiro Kato,^{1,37} Shaohua Fan,⁷ Akinori Kawakami,¹ Yusuke Suita,¹ Kazumasa Wakamatsu,⁸ Vivien Igras,¹ Jianming Zhang,⁹ Paula P. Navarro,^{10,11} Camila Makhoulouta Lugo,^{10,11} Haley R. Noonan,⁶ Kathleen A. Christie,^{12,13} Kaspar Itin,¹⁴ Nisma Mujahid,^{1,15,16} Jennifer A. Lo,¹ Chong Hyun Won,¹⁷ Conor L. Evans,¹⁸ Qing Yu Weng,¹ Hequn Wang,¹⁸ Sam Osseiran,¹⁸ Alyssa Lovas,¹⁸ István Németh,¹⁹ Antonio Cozzio,²⁰ Alexander A. Navarini,¹⁴ Jennifer J. Hsiao,¹

(Author list continued on next page)

¹Cutaneous Biology Research Center, Department of Dermatology, Massachusetts General Hospital, Harvard Medical School, Charlestown, MA 02129, USA

²School of Mathematics and Statistics, The Open University, Milton Keynes, MK7 6AA, UK

³Department of Genetics, Evolution and Environment and UCL Genetics Institute, University College London, London WC1E 6BT, UK

⁴Department of Dermatology, Erasmus Medical Center, 3015 Rotterdam, the Netherlands

⁵Department of Dermatology and Cutaneous Biology Research Institute, Yonsei University College of Medicine, 03722 Seoul, Korea

⁶Stem Cell Program and Division of Hematology/Oncology, Boston Children's Hospital and the Howard Hughes Medical Institute, Boston, MA 02115, USA

⁷State Key Laboratory of Genetic Engineering, Human Phenome Institute, School of Life Sciences, Fudan University, 200438 Shanghai, China

⁸Institute for Melanin Chemistry, Fujita Health University, Toyoake, Aichi 470-1192, Japan

⁹National Research Center for Translational Medicine (Shanghai), State Key Laboratory of Medical Genomics, Ruijin Hospital, Shanghai Jiao Tong University School of Medicine, 200025 Shanghai, China

¹⁰Department of Molecular Biology, Massachusetts General Hospital, Boston, MA 02114, USA

¹¹Department of Genetics, Harvard Medical School, Boston, MA 02115, USA

¹²Center for Genomic Medicine and Department of Pathology, Massachusetts General Hospital, Boston, MA 02114, USA

¹³Department of Pathology, Harvard Medical School, Boston, MA 02115, USA

¹⁴Department of Dermatology, University Hospital of Basel, 4031 Basel, Switzerland

¹⁵Boston University School of Medicine, Boston, MA 02118, USA

(Affiliations continued on next page)

SUMMARY

Ultraviolet (UV) light and incompletely understood genetic and epigenetic variations determine skin color. Here we describe an UV- and microphthalmia-associated transcription factor (MITF)-independent mechanism of skin pigmentation. Targeting the mitochondrial redox-regulating enzyme nicotinamide nucleotide transhydrogenase (NNT) resulted in cellular redox changes that affect tyrosinase degradation. These changes regulate melanosome maturation and, consequently, eumelanin levels and pigmentation. Topical application of small-molecule inhibitors yielded skin darkening in human skin, and mice with decreased NNT function displayed increased pigmentation. Additionally, genetic modification of NNT in zebrafish alters melanocytic pigmentation. Analysis of four diverse human cohorts revealed significant associations of skin color, tanning, and sun protection use with various single-nucleotide polymorphisms within *NNT*. NNT levels were independent of UVB irradiation and redox modulation. Individuals with postinflammatory hyperpigmentation or lentigenes displayed decreased skin NNT levels, suggesting an NNT-driven, redox-dependent pigmentation mechanism that can be targeted with NNT-modifying topical drugs for medical and cosmetic purposes.

INTRODUCTION

Pigmentation of human skin, which confers protection against skin cancer, evolved over one million years ago in the setting of evolutionary loss of body hair (Jablonski and Chaplin, 2017).

Human skin color results from relative amounts of yellow-orange pheomelanin and black-brown eumelanin (Del Bino et al., 2015). Darker-pigmented individuals are more protected from oncogenic UV radiation by the light-scattering and antioxidant properties of eumelanin (Jablonski and Chaplin, 2012).



Nhu Nguyen,¹ Lajos V. Kemény,^{1,21} Othon Iliopoulos,²² Carola Berking,²³ Thomas Ruzicka,²⁴ Rolando Gonzalez-José,²⁵ Maria-Cátira Bortolini,²⁶ Samuel Canzales-Quinteros,²⁷ Victor Acuna-Alonso,²⁸ Carla Gallo,²⁹ Giovanni Poletti,²⁹ Gabriel Bedoya,³⁰ Francisco Rothhammer,^{31,32} Shosuke Ito,⁸ Maria Vittoria Schiaffino,³³ Luke H. Chao,^{10,11} Benjamin P. Kleinstiver,^{12,13} Sarah Tishkoff,³⁴ Leonard I. Zon,⁶ Tamar Nijsten,⁴ Andrés Ruiz-Linares,^{35,36} David E. Fisher,^{1,22,40,41,*} and Elisabeth Roider^{1,14,19,40,42,*}

¹⁶University of Utah, Department of Dermatology, Salt Lake City, UT 84132, USA

¹⁷Department of Dermatology, Asan Medical Center, Ulsan University College of Medicine, 05505 Seoul, Korea

¹⁸Wellman Center for Photomedicine, Massachusetts General Hospital, Harvard Medical School, Charlestown, MA 02129, USA

¹⁹Department of Dermatology and Allergology, University of Szeged, 6720 Szeged, Hungary

²⁰Department of Dermatology, Venerology, and Allergology, Kantonsspital St. Gallen, 9007 St. Gallen, Switzerland

²¹Department of Dermatology, Venereology, and Dermatocarcinology, Semmelweis University, 1085 Budapest, Hungary

²²Massachusetts General Hospital Cancer Center, Harvard Medical School, Boston, MA 02114, USA

²³Department of Dermatology, Universitätsklinikum Erlangen, Friedrich Alexander University Erlangen-Nürnberg, 91054, Erlangen, Germany

²⁴Department of Dermatology and Allergy, University Hospital Munich, Ludwig Maximilian University, 80337 Munich, Germany

²⁵Instituto Patagónico de Ciencias Sociales y Humanas-Centro Nacional Patagónico, CONICET, Puerto Madryn U9120ACD, Argentina

²⁶Departamento de Genética, Universidade Federal do Rio Grande do Sul, Porto Alegre 91501-970, Brazil

²⁷Unidad de Genómica de Poblaciones Aplicada a la Salud, Facultad de Química, Universidad Nacional Autónoma de México e Instituto Nacional de Medicina Genómica, Mexico City 04510, Mexico

²⁸National Institute of Anthropology and History, Mexico City 4510, Mexico

²⁹Laboratorios de Investigación y Desarrollo, Facultad de Ciencias y Filosofía, Universidad Peruana Cayetano Heredia, Lima 15102, Peru

³⁰Genética Molecular (GENMOL), Universidad de Antioquia, Medellín 5001000, Colombia

³¹Instituto de Alta Investigación, Universidad de Tarapacá, Arica 1000009, Chile

³²Programa de Genética Humana, ICBM, Facultad de Medicina, Universidad de Chile, Santiago 1027, Chile

³³Internal Medicine, Diabetes and Endocrinology Unit, IRCCS San Raffaele Scientific Institute, Milan 20132, Italy

³⁴Departments of Genetics and Biology, University of Pennsylvania, Philadelphia, PA, USA

³⁵Ministry of Education Key Laboratory of Contemporary Anthropology and Collaborative Innovation Center of Genetics and Development, School of Life Sciences and Human Phenome Institute, Fudan University, Shanghai 200433, China

³⁶UMR 7268, CNRS-EFS-ADES, Aix-Marseille University, Marseille 13005, France

³⁷Department of Immunology, Center for 5D Cell Dynamics, Nagoya University Graduate School of Medicine, Nagoya 466-8550, Japan

³⁸These authors contributed equally

³⁹These authors contributed equally

⁴⁰These authors contributed equally

⁴¹Senior author

⁴²Lead contact

*Correspondence: dfisher3@mgh.harvard.edu (D.E.F.), eroider@cbr2.mgh.harvard.edu (E.R.)

<https://doi.org/10.1016/j.cell.2021.06.022>

Pigment dictates how light is absorbed and disseminated in skin (Pathak et al., 1962). UV light can interact photochemically with DNA to form cyclobutane pyrimidine dimers (CPD) and 6-4 photoproducts and causes production of reactive oxygen species (ROS) through multiple mechanisms, increasing the risk of skin cancer (Premi et al., 2015). Although eumelanin has antioxidant activity, ROS-mediated oxidation of DNA bases and lipid peroxidation are elevated in mice that produce pheomelanin only (Mitra et al., 2012).

Melanocytes produce melanin within subcellular organelles called melanosomes that mature from early, unpigmented (stages I–II) toward late, pigmented states (stages III–IV). Early-stage melanosomes are recognized by proteinaceous fibrils within the melanosomal lumen. In the late stages, melanin is deposited gradually on the fibrils (Raposo and Marks, 2007). These mature melanosomes are ultimately transferred to keratinocytes (Park et al., 2009), where they coalesce in a supranuclear location on the sun-facing side. UV radiation triggers tanning through p53-mediated induction of POMC (proopiomelanocortin) peptides in keratinocytes, leading to MC1R activation on melanocytes and cyclic AMP (cAMP)-mediated induction of the microphthalmia-associated transcription factor (*MITF*), which induces expression of tyrosinase-related protein 1 and 2 (*TYRP1* and *DCT*) (Lo and

Fisher, 2014) and tyrosinase, which drive melanosome maturation (Paterson et al., 2015) and increased production of eumelanin (Iozumi et al., 1993).

The enzyme nicotinamide nucleotide transhydrogenase (NNT) is located in the inner mitochondrial membrane. It regulates mitochondrial redox levels by coupling hydride transfer between β -nicotinamide adenine dinucleotide NAD(H) and β -nicotinamide adenine dinucleotide 2'-phosphate NADP (+) to proton translocation across the inner mitochondrial membrane (Earle and Fisher, 1980; Rydström et al., 1970; Zhang et al., 2017). Even though The Human Protein Atlas (<http://www.proteinatlas.org>; Uhlén et al., 2015) showed expression of NNT in human melanocytes, fibroblasts, keratinocytes, and other epidermal cells, so far NNT has not been described to be involved in mechanisms of direct regulation of skin pigment. Here we report a role of NNT in modulating melanosome maturation and pigmentation.

RESULTS

NNT enables regulation of pigmentation by changing intracellular redox levels

NNT was depleted using a pool of small interfering RNAs (siRNAs; siNNT) in the human melanoma cell lines UACC257

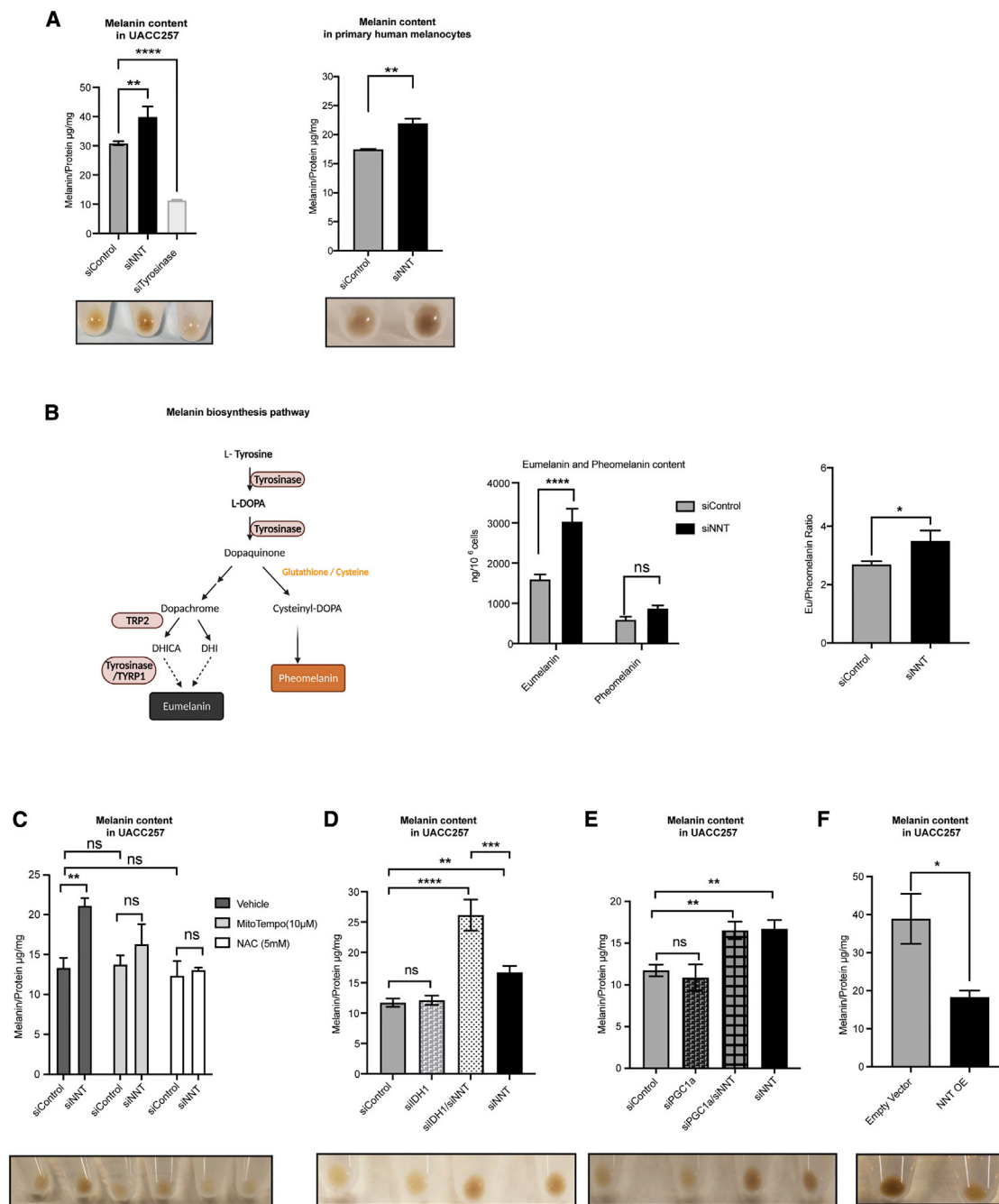


Figure 1. Nicotinamide nucleotide transhydrogenase (NNT) regulates *in vitro* pigmentation via a redox-dependent mechanism

(A) siNNT increases pigmentation. Shown is quantification of intracellular melanin content of UACC257 cells treated with siControl, siNNT, or siTyrosinase for 72 h (left panel) and human primary melanocytes treated with siControl or siNNT for 96 h (right panel); $n = 3$, analyzed by ordinary one-way ANOVA with Dunnett's post-test (left panel) and unpaired, two-sided t test (right panel). Below the graphs, representative cell pellets of the indicated treatment (1×10^6 cells).

(B) Schematic of the pathways of pheomelanin and eumelanin biosynthesis. DHICA, 5,6-dihydroxyindole-2-carboxylic acid; DHI, 5,6-dihydroxyindole. UACC257 melanoma cells were treated with siControl or siNNT for 5 days, and eumelanin and pheomelanin were measured using HPLC techniques ($n = 3$). Absolute pigment levels (left graph) were analyzed by ordinary two-way ANOVA. The eumelanin/pheomelanin ratio (right graph) was analyzed by unpaired Student's t test.

(C) siNNT-induced increased pigmentation of human UACC257 melanoma cells is blocked by NAC (5 mM) or MitoTEMPO (20 μM) (daily treatment for 72 h); $n = 3$, analyzed by ordinary two-way ANOVA with Šidák's post-test.

(legend continued on next page)

and SK-MEL-30 and in primary human melanocytes. In all three cell models, knockdown of NNT led to a significant increase in melanin content (Figures 1A and S1A–S1D). The increase in pigmentation following siNNT was blocked by simultaneous knockdown of tyrosinase, demonstrating the dependence of siNNT-mediated pigmentation on tyrosinase (Figure S1A).

NNT has been described to increase glutathione (GSH) in *Nnt* wild-type versus *Nnt* mutant C57BL/6J mice (Ronchi et al., 2013) as well as in human myocardium (Sheeran et al., 2010). In line with this, silencing NNT caused a decrease in the GSH/GSSG ratio in UACC257 human melanoma cells (Figure S1E). Cysteine or reduced GSH is a required component for pheomelanin synthesis (Ito and IFPCS, 2003; Jara et al., 1988; Figure 1B, schematic), suggesting that NNT may modulate pigmentation via its role in regenerating GSH and thereby affect the pheomelanin-to-eumelanin ratio. To investigate this possibility, high-performance liquid chromatography (HPLC) was utilized and demonstrated significantly increased absolute levels of eumelanin, but not pheomelanin, upon NNT knockdown (Figure 1B, left graph). The eumelanin-to-pheomelanin ratio also showed a significant increase (Figure 1B, right graph). Tyrosinase silencing was used as a positive control, showing efficient and quick depigmentation 5 days after transfection (Figure 1A), resulting in decreased levels of eumelanin and pheomelanin and, as suspected, no significant change in the eumelanin-to-pheomelanin ratio (Figure S1F). These data suggest that NNT modulates melanin synthesis toward a eumelanin phenotype.

Because NNT's essential role as an antioxidant enzyme against ROS by controlling the NADPH conversion, we hypothesized that the increase in pigmentation following silencing of NNT is driven by an oxidative stress-dependent mechanism. As expected, knockdown of NNT caused a significant increase in the NADP/NADPH ratio (Figure S1E) and induced cytosolic ROS (Figure S1G) in UACC257 cells. Adding the thiol antioxidant *N*-acetylcysteine (NAC), the mitochondrion-targeted antioxidant MitoTEMPO, or NADPH to siNNT inhibited the siNNT-mediated increase in pigmentation (Figures 1C, S1A, and S1H), demonstrating the dependence of siNNT-mediated pigmentation on oxidative stress.

To understand how cytosolic and mitochondrial oxidative stress levels are connected, isocitrate dehydrogenase 1 (IDH1), a source of cytosolic NADPH (Zhao and McAlister-Henn, 1996), was depleted in UACC257 cells (Figures 1D, S1I, and S1J). Interestingly, although siNNT alone increased pigmentation, siIDH1 alone had no significant effect on pigmentation (Figure 1D). However, double knockdown of NNT and IDH1 increased the intracellular melanin content further, exceeding the siNNT induction of pigmentation (Figure 1D). To exclude the possibility that siIDH1 or siIDH1-induced oxidative stress may increase NNT levels, NNT mRNA levels were measured (Figures S1I and S1J), which showed no changes. To understand

whether cytosolic ROS may be the driver of the observed pigmentation change, cytosolic oxidative stress was measured upon silencing of siNNT and siIDH1 (Figure S1G), showing similar effects of the different siRNAs, emphasizing the crucial role of NNT in human pigmentation.

To clarify the role of mitochondrial oxidative stress, we investigated the participation of peroxisome proliferator-activated receptor gamma coactivator 1-alpha (PGC1 α). As shown previously, intramitochondrial concentrations of ROS were increased significantly in PGC1 α -depleted melanoma cells, associated with decreased levels of reduced GSH, cystathionine, and 5-adenosylhomocysteine (Vazquez et al., 2013). However, no change in pigmentation was detected in PGC1 α -depleted human UACC257 melanoma cells (Figures 1E and S1J), emphasizing the specific role of NNT and especially NNT-induced cytosolic oxidative stress in the pigmentation response. Finally, overexpression of NNT in UACC257 cells (Figure S1K) increased GSH/GSSG ratios and decreased NADP/NADPH ratios (Figure S1L). As opposed to the increase in pigmentation observed with silencing of NNT, overexpression of NNT induced a significant decrease in pigmentation (Figure 1F), confirming the relationship between NNT and pigmentation in both directions.

Our data suggest that NNT affects pigmentation via a redox-dependent mechanism.

NNT depletion enhances pigmentation independent of the classic cAMP-MITF-pigmentation pathway

To elucidate the mechanism underlying hyperpigmentation after NNT knockdown, we investigated its effects on key melanin biosynthesis factors in UACC257 cells (Figure 2A). NNT knockdown revealed a significant increase in the levels of the melanin biosynthesis enzymes tyrosinase, TYRP1, and TRP2/DCT (Figure 2A). In addition, tyrosinase activity was increased upon silencing of siNNT (Figure S2A). Because MITF is the main regulator of these enzymes and the master regulator of melanogenesis (Figures S2B–S2G), we measured MITF protein levels and its transcriptional activity. Upon silencing of NNT, neither MITF protein levels nor mRNA levels were changed significantly (Figures S2C and S2D). Furthermore, MITF promoter activity was decreased modestly following siNNT (Figures S2E and S2F), whereas no significant changes in the mRNA levels of TYRP1, TRP2/DCT, or tyrosinase were observed (Figures S2G). This suggests that NNT can affect tyrosinase, TRP2/DCT, and TYRP1 protein levels without affecting their mRNA levels. Because cAMP is a crucial messenger in UV light-induced skin pigmentation (the “classic cAMP-MITF-pigmentation pathway”; Figure S2B), baseline cAMP levels in siControl- versus siNNT-transfected UACC257 cells were assayed and found to be unaffected by siNNT (Figure S2H). Treatment of primary human melanocytes with forskolin, an activator of adenylate cyclase, which increases cAMP levels, did not affect NNT expression levels

(D and E) Quantification of intracellular melanin content of UACC257 cells treated for 72 h with siControl, siNNT, siIDH1, or siIDH1 + siNNT (D) or with siControl, siNNT, siPGC1 α , or siNNT + siPGC1 α (E); n = 3, analyzed by ordinary one-way ANOVA with Dunnett's post-test. Shown below the graphs are representative cell pellets (1×10^6 cells) of the indicated treatments.

(F) OE of NNT reduced pigmentation. Shown is melanin content in UACC257 cells that overexpressed NNT (NNT OE) or the corresponding control (empty vector) for 12 days; n = 3, analyzed by unpaired, two-sided t test.

All data are expressed as mean \pm SEM; *p < 0.05, **p < 0.01, ****p < 0.0001.

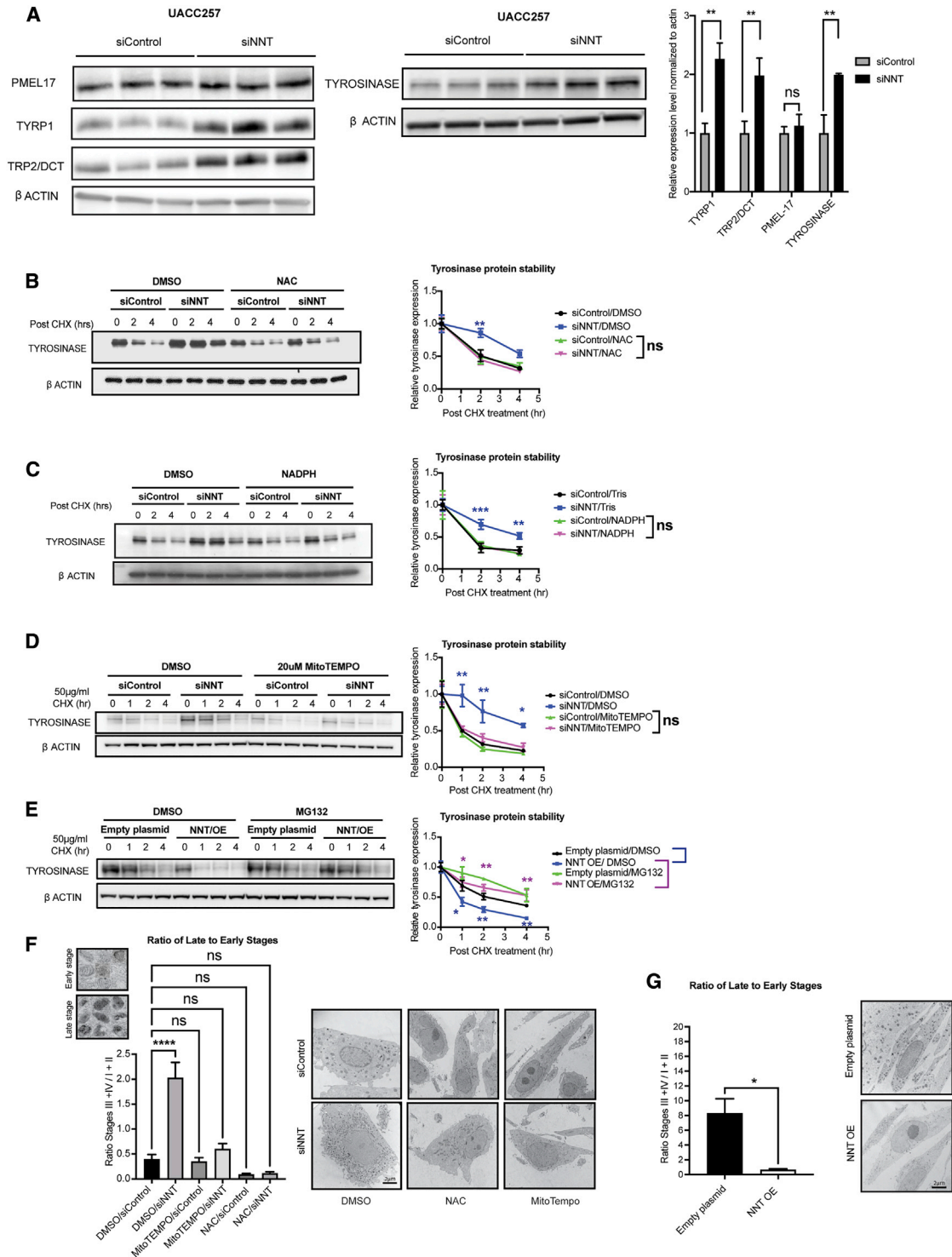


Figure 2. Inhibition of NNT enhances melanosome maturation and tyrosinase protein stability via a redox-dependent mechanism

(A) Immunoblot analysis of whole-cell lysates from UACC257 melanoma cells 72 h after treatment with siControl or siNNT, showing increased tyrosinase, DCT/ TRP2, and TYRP1 but not PMEL17 protein levels. Band intensities were quantified by ImageJ, normalized to β -actin, plotted relative to siControl ($n = 3$), and analyzed by multiple t tests with Holm-Sidak post-test.

(B–D) siNNT-mediated increased protein stability is blocked by antioxidants. UACC257 cells transfected with siControl or siNNT were treated 24 h after transfection with 5 mM NAC (B), 0.1 mM NADPH (C), 20 μ M MitoTEMPO (D), or control vehicle for 48 h, followed by CHX treatment. Cells were harvested 0, 1, 2,

(legend continued on next page)

(Figure S2I), nor did UVB irradiation of human skin (Figure S2J). In addition, no increase in POMC (Figure S2G) or p53 (Figure S2K) was observed in UACC257 cells upon siNNT treatment. Modulating the general redox system by adding NAC, MitoTEMPO, or H₂O₂ did not affect NNT protein levels (Figure S2L).

Finally, overexpression of NNT in UACC257 cells showed a significant decrease in tyrosinase protein levels (Figure S2M) but not its mRNA levels (Figure S2N).

These data suggest the existence of an NNT-dependent pigmentation mechanism independent of the previously established cAMP-MITF-dependent pigmentation pathway.

NNT promotes ubiquitin-proteasome-dependent tyrosinase degradation and modulates melanosome maturation

Because altering NNT was found to affect the protein levels of tyrosinase and related key melanogenic enzymes (Figure 2A) without affecting their mRNA levels (Figure S2G), we hypothesized that NNT can affect the stability of certain melanosomal proteins. The effect of NNT-mediated redox changes on tyrosinase protein stability was investigated by knockdown of *NNT* mRNA in the presence or absence of an antioxidant, followed by inhibition of protein synthesis with cycloheximide (CHX) and measurements of the rate of decay of tyrosinase protein. Silencing of *NNT* significantly increased tyrosinase protein stability, and this effect was prevented by antioxidant treatment with NAC, NADPH, or MitoTEMPO (Figures 2B–2D).

The mechanism of tyrosinase degradation is not fully understood, although it has been shown that tyrosinase is degraded via the ubiquitin-proteasome system (Bellei et al., 2010). Addition of carbobenzoxy-L-leucyl-L-leucyl-L-leucinal (MG132), a cell-permeable, reversible proteasome inhibitor, prevented an NNT overexpression-induced decrease in Tyrosinase protein stability in UACC257 cells (Figure 2E), suggesting that NNT induces changes in melanin levels through proteasome-mediated degradation of Tyrosinase protein.

Because siNNT-induced increases in melanogenesis enzymes, NNT's role in NADPH and GSH generation, and its location in the inner mitochondrial membrane, we hypothesized that NNT function might be connected to maturation of melanosomes. The effects of modulating NNT expression on the ultrastructure of melanosomes was assessed by electron microscopy in primary human melanocytes. Knockdown of NNT resulted in a striking increase in late-stage/pigmented melanosomes (stages III and IV) (Figures 2F and S3A), whereas overexpression of NNT resulted in a switch toward early-stage/unpigmented melanosomes (stages I and II) (Figure 2G), establishing

a role for NNT in regulating melanosome maturation. In line with the pigmentation data (Figure 1C), cotreatment with NAC or MitoTEMPO prevented the siNNT-induced phenotype (Figures 2F and S3A). The absolute number of melanosomes per cytosolic area was not affected by NNT knockdown or overexpression (Figure S3B), which is in line with the observation that the pre-melanosome protein Pmel17, a marker for early melanosome development, did not change upon depletion of NNT (Figure 2A). Our data suggest that inhibition of NNT drives pigmentation by stabilizing tyrosinase and possibly other tyrosinase-related proteins (TYRP1 and TRP2/DCT) associated with increased melanosome maturation.

Previously, it has been shown that mitochondria are connected with melanosomes via physical contact, requiring Mitofusin-2 (MFN2) (Daniele et al., 2014). The connection between these two organelles may enable localized interorganellar exchange (Daniele et al., 2014; Wu and Hammer, 2014). To understand whether siNNT-induced pigmentation may rely on an equivalent mechanism, we performed simultaneous knockdown of NNT and MFN2 in UACC257 cells (Figure S3G) and in human primary melanocytes (Figure S3H). Consistent with previous findings (Daniele et al., 2014), evaluation of mitochondrion-melanosome proximities by electron microscopy confirmed that knockdown of MFN2 resulted in a strong decrease in close appositions (<20 nm) compared with the control (Figure S3C). By contrast, silencing of NNT alone led to a relative increase of organelle contiguities, possibly related to the stimulation of melanogenesis (Figure S3C), and double knockdown prevented this increase (Figure S3C), whereas melanosome and mitochondrion numbers remained unchanged (Figures S3D and S3E). Similar to melanosome-mitochondrion proximity, silencing of NNT in UACC257 human melanoma cells significantly increased the intracellular melanin content, which was reversed by simultaneous knockdown of NNT and MFN2 (Figure S3F). Finally, overexpression of NNT resulted in a decrease in close appositions (<20 nm) compared with the control (Figure S3C), whereas no change was observed in melanosome and mitochondrion numbers (Figures S3B and S3E).

Although these findings suggest that MFN2 and melanosome-mitochondrion proximity may contribute to NNT regulation of pigmentation changes, the role of MFN2 in melanogenesis is complex. In addition to interorganellar connections, MFN2 regulates many functions in cells, including mitochondrial fusion, ATP production, and autophagy, that may affect pigmentation (Filadi et al., 2018). In particular, MFN2 deficiency has been associated with impaired autophagic degradation and accumulation of autophagosomes (Zhao et al., 2012; Sebastián et al., 2016).

and 4 h after CHX treatment for immunoblotting. Band intensities were quantified by ImageJ, normalized to β -actin, and plotted relative to $t = 0$; $n = 3$, analyzed by repeated-measures two-way ANOVA with Sidák's post-test (asterisks indicate significance of siControl/vehicle versus each of the other three groups).

(E) The proteasome inhibitor MG132 inhibits tyrosinase protein degradation upon CHX treatment of NNT-overexpressing UACC257 cells. The cells were treated with DMSO or MG132 (10 μ M) for 6 h, followed by CHX treatment for 0, 1, 2, and 4 h and immunoblotting. Band intensities were quantified by ImageJ, normalized to β -actin, and plotted relative to $t = 0$; $n = 3$, analyzed by repeated-measures two-way ANOVA with Sidák's post-test.

(F) Enhanced melanosome maturation induced by siNNT in primary human melanocyte cells is blocked by NAC (5 mM) or MitoTEMPO (20 μ M) (daily treatment for 96 h). The ratios of late stages (III + IV) to early stages (I + II) are presented. $n = 4$ –5, analyzed by ordinary two-way ANOVA with Sidák's post-test.

(G) Inhibition of melanosome maturation induced by NNT OE in primary human melanocytes for 7 days. The ratios of late- to early-stage melanosomes were compared by unpaired, two-sided t test; $n = 4$ (NNT OE) and $n = 8$ (empty plasmid).

All data are expressed as mean \pm SEM. * $p < 0.05$, ** $p < 0.01$, *** $p < 0.001$, **** $p < 0.0001$.

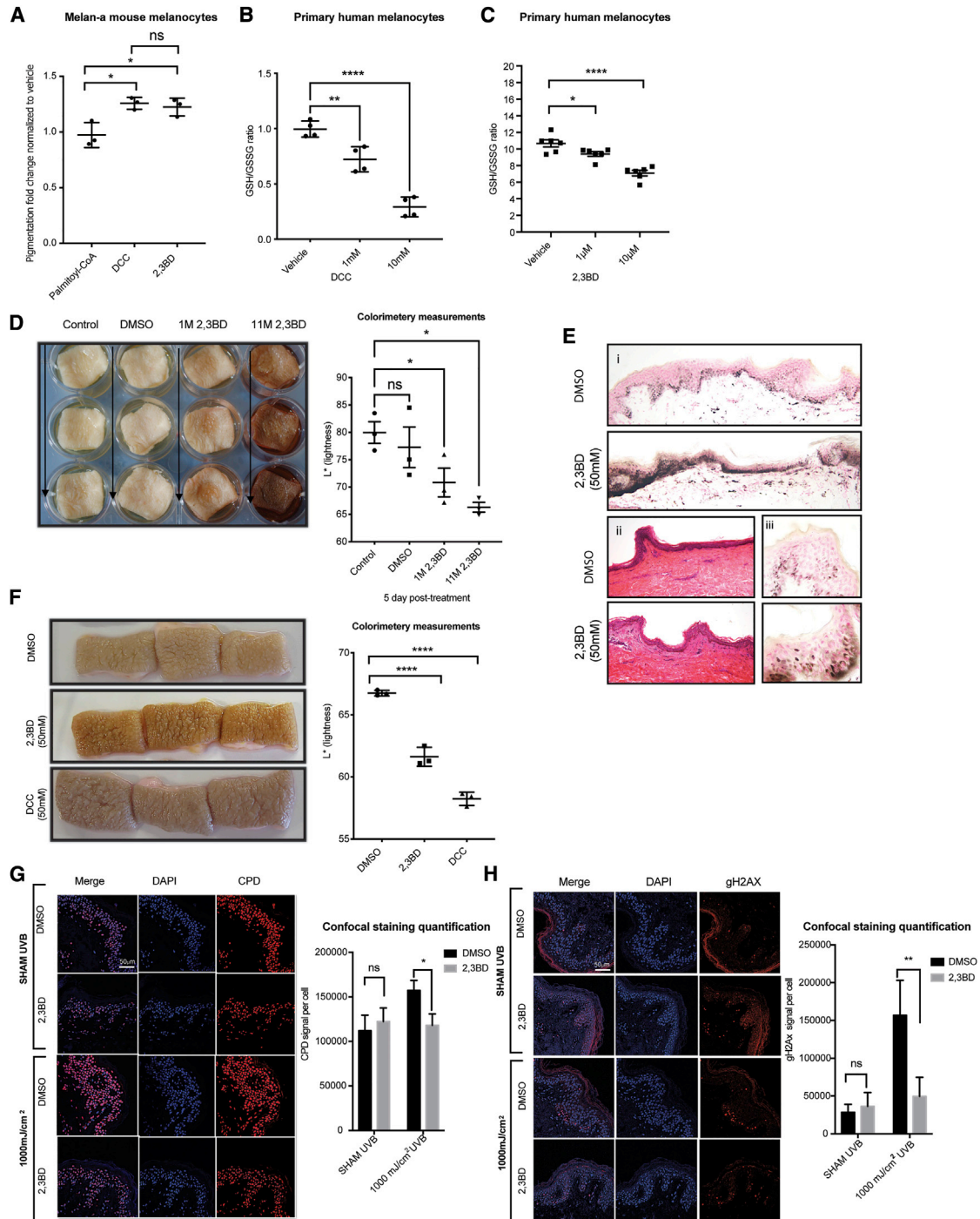


Figure 3. NNT inhibitors are non-toxic and induce pigmentation of primary melanocytes *in vitro* and in human skin explants

(A) Murine melanocytes (Melan-A) showed increased melanin content after incubation with 2 mM 2,3BD or DCC but not after incubation with palmitoyl-CoA; $n = 3$, analyzed by ordinary one-way ANOVA with Dunnett's post-test.

(B and C) Treatment of primary human melanocytes with different doses of DCC (B, $n = 4$) or 2,3BD (C, $n = 6$) for 24 h yielded decreased GSH/GSSG ratios; analyzed by ordinary one-way ANOVA with Tukey's (B) or Dunnett's (C) post-test.

(D) A single, one-time topical treatment with 2,3BD (1 M or 11 M) induces human skin pigmentation after 5 days. Left panel: representative images of at least three individual experiments. Right panel: reflective colorimetry measurements of skin treated with 2,3BD (higher L^* values represent lighter skin tones); $n = 3$, analyzed by ordinary one-way ANOVA with Dunnett's post-test.

(legend continued on next page)

Consistent with those findings, knockdown of MFN2 in human primary melanocytes and UACC257 cells resulted in the presence of large autophagosome-like structures containing numerous and partly intact melanosomes (Figure S3I) as well as increased LCB3 type II (Figure S3J), which can be associated with enhanced autophagosome synthesis or reduced autophagosome degradation (Barth et al., 2010). Because defects in autophagosome formation and turnover interfere with melanosome biogenesis and are associated with pigmentary defects (Ho and Ganesan, 2011), we conclude that MFN2 can regulate pigmentation via distinct but incompletely understood pathways.

Topical NNT inhibitors increase pigmentation

Currently, only a few topical drugs are capable of altering pigmentation in human skin (Rendon and Gaviria, 2005). No topical skin darkeners are available for clinical use. Systemic administration of peptides, such as α -MSH (melanocyte-stimulating hormone) analogs (e.g., melanotan), has been used to successfully increase skin pigmentation (Ugwu et al., 1997). Three NNT inhibitors (*N,N'*-dicyclohexylcarbodiimide [DCC], 2,3-butanedione [2,3BD], and palmitoyl-coenzyme A [CoA]) have been described previously (Figure S4A; Rydström, 1972). DCC is commonly used as a peptide-coupling reagent, and 2,3BD is used as a flavoring agent (Rigler and Longo, 2010). Both are low-molecular-weight compounds (DCC, 206.33 g/mol; 2,3BD, 86.09 g/mol) potentially capable of penetrating the human epidermis. Palmitoyl-CoA, like 2,3BD, is a natural product but has a high molecular weight (1005.94 g/mol), making skin penetration challenging. The effects of all three compounds on pigmentation of intermediately pigmented murine Melan-A cells (Figure 3A) were assessed. 2,3BD and DCC significantly increased the melanin content in intermediately pigmented murine Melan-A cells (Figure 3A) and in human primary melanocytes (Figure S4D). *In vitro* toxicity was assessed in primary human melanocytes, dermal fibroblasts, and keratinocytes (Figure S4B and S4C), showing no significant toxicity in doses up to 10 μ M. To verify the effects of the small-molecular-weight compounds on NNT function, the GSH/GSSG ratio, an indirect endpoint of NNT enzyme activity, was measured, revealing decreased GSH/GSSG ratios induced by DCC and 2,3BD in primary melanocytes (Figures 3B and 3C) and by DCC in UACC257 melanoma cells (Figure S4E) without significant toxicity (Figures S4C and S4E). Treatment of primary human melanocytes with siNNT or 2,3BD significantly increased the intracellular melanin content, but simultaneous treatment with siNNT and 2,3BD did not further increase the melanin (Figure S4D), suggesting that

enhancement of pigmentation by 2,3BD may be mediated by inhibition of NNT.

Next we tested the compounds on human skin explants from different skin types. As suggested above, palmitoyl-CoA did not penetrate the epidermis and had no effect on pigmentation (data not shown). In abdominal skin from individuals of fair skin (phototype 1–2), 2,3BD yielded strong induction of pigmentation at relatively high doses (Figure 3D). Histology with Fontana-Masson staining showed increased melanin in 2,3BD-treated skin (Figures 3Ei and S4F) and no obvious cell damage or inflammation by H&E staining (Figure 3Eii), although the volatility of 2,3BD produces a strong butter-like aroma, potentially limiting its future clinical use. Importantly, keratinocytic supranuclear caps (Figures 3Eiii and S4F) were present, suggesting formation of functional melanosome/melanin transfer to keratinocytes, which allows cells to protect their nuclei from UV radiation. Daily application of 50 mM 2,3BD or DCC on skin from intermediately pigmented (type 3–4) individuals yielded significantly increased pigmentation after 5 days (Figure 3F). Because of the activity of DCC as a coupling agent and its corresponding unclear toxicity risks, only 2,3BD was used in subsequent experiments.

2,3BD-induced skin pigmentation can prevent UVB-induced DNA damage

UV radiation interacting with DNA can directly produce CPDs and 6–4 photoproducts, whereas ROS-mediated DNA modifications produce alternative nucleotide adducts, including 8,5-cyclo-2-deoxyadenosine, 8,5-cyclo-2-deoxyguanosine, and 8-oxo-deoxyguanine (Jaruga and Dizdaroglu, 2008; Wang, 2008).

Although superficial epidermal cells containing modified proteins, lipids, and DNA are shed continuously through corneocyte desquamation, durable basal cells require active DNA repair machinery for their maintenance. Melanomas have been found to contain high frequencies of somatic mutations with characteristic UV-induced signatures of C-to-T and G-to-A transitions (Berger et al., 2012). Protecting human skin from these intermediates is a major goal of skin cancer prevention strategies. As shown in previous studies, increased pigmentation can help to protect against CPD formation (D'Orazio et al., 2006; Mujahid et al., 2017). We tested whether 2,3BD-induced pigmentation can protect skin from UVB-induced CPD formation. After inducing a visible increase in pigmentation of human skin by application of 50 mM 2,3BD to skin type 2–3 for 5 days (Figure 3G), UVB was applied, and CPD formation was detected by immunofluorescence staining and normalized to the total number of cells. It was observed that 2,3BD treatment protected

(E) Fontana-Masson staining of melanin in human skin after (i) 2,3BD (50 mM) and (ii) hematoxylin and eosin staining compared with vehicle control (DMSO) and (iii) supranuclear capping in human keratinocytes of 2,3BD- and vehicle control-treated skin displayed by Fontana-Masson staining.

(F) The NNT inhibitors 2,3BD or DCC, applied daily at a 50 mM dose, resulted in skin darkening after 5 days. Left panel: representative images of three individual experiments. Right panel: reflective colorimetry measurements of human skin treated with 2,3BD, DCC, or DMSO vehicle (higher L^* values represent lighter skin tones); $n = 3$, analyzed by ordinary one-way ANOVA with Dunnett's post-test.

(G) Immunofluorescence staining for CPD formation (red) in human skin treated with 50 mM 2,3BD for 5 consecutive days. On the last day, skin was irradiated with 1,000 mJ/cm² UVB. The results show a protective role of 2,3BD from UVB-induced CPD damage. Representative images of three individual experiments are displayed. Scale bar, 50 μ m. Quantified results were normalized to the total number of cells; $n = 3$, analyzed by ordinary two-way ANOVA with Sidák's post-test.

(H) Measurement of γ -H2AX (red) in human skin revealed no significant toxicity of 2,3BD, whereas 2,3BD-induced pigmentation protected from UVB-induced γ -H2AX formation. Representative images of three individual experiments are displayed. Scale bar, 50 μ m. Quantified results were normalized to the total number of cells; $n = 3$, analyzed by ordinary two-way ANOVA with Sidák's post-test.

All data are expressed as mean \pm SEM. * $p < 0.05$, ** $p < 0.01$, *** $p < 0.001$, **** $p < 0.0001$.

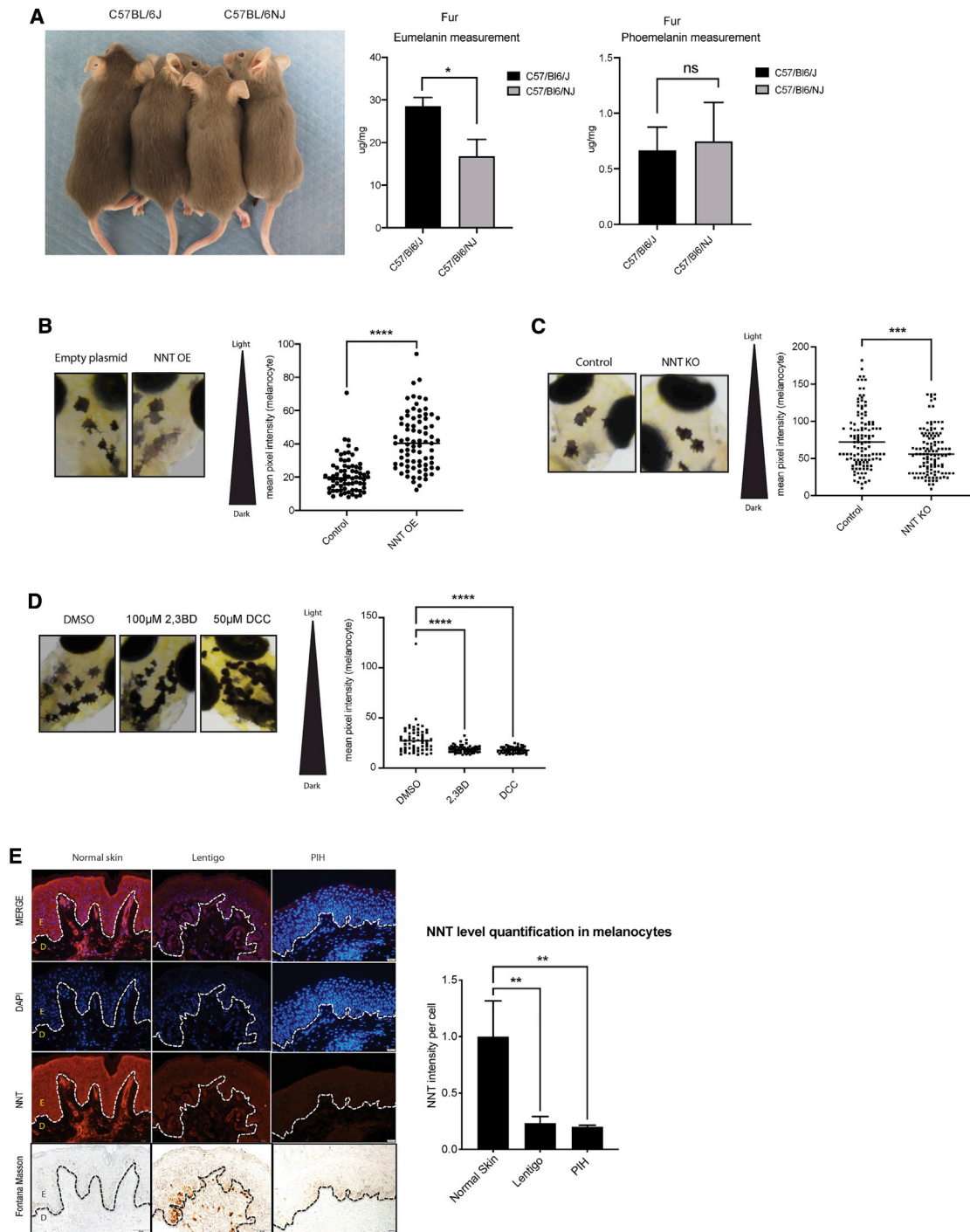


Figure 4. NNT regulates pigmentation in mice, zebrafish, and human pigmentation disorders

(A) Left panel: C57BL/6J mice carrying a 5-exon deletion in the *Nnt* gene, resulting in homozygous loss of NNT activity, display increased fur pigmentation compared with C57BL/6NJ wild-type *Nnt* animals. Right graphs: mouse fur samples were analyzed for pheomelanin and eumelanin levels by HPLC. $n = 3$, analyzed by multiple t tests with Holm-Šidák post-test.

(B) Left panel: zebrafish overexpressing NNT (NNT OE) display decreased pigmentation in individual melanocytes after 5 days. A representative image is displayed. Results of mean melanocytic brightness, quantified by pixel-based analysis, are shown in the graph on the right. Empty plasmid ($n = 11$ fish, 72 melanocytes), NNT OE ($n = 12$ fish, 78 melanocytes), analyzed by unpaired, two-sided t test.

(legend continued on next page)

against formation of UVB-induced CPD (Figure 3G). We then measured γ -H2AX, a marker of DNA double-stranded breaks, to investigate potential 2,3BD-mediated toxicity as well as whether 2,3BD-mediated skin pigmentation could protect from UVB-induced γ -H2AX induction (Figure 3H). 2,3BD was observed to be non-toxic, and the pigmentation it produced could protect human skin from UVB-induced γ -H2AX induction.

NNT regulates pigmentation in mice, zebrafish, and human pigmentation disorders

C57BL/6J and C57BL/6NJ mice are substrains of the C57BL/6 mouse with known genetic differences. Although C57BL/6NJ mice are homozygous for the *Nnt* wild-type allele, C57BL/6J mice are homozygous for the *Nnt*C57BL/6J mutation. This mutant allele is missing a stretch of 17,814 bp between exons 6 and 12, resulting in a lack of mature protein in these mutants (Toye et al., 2005; Huang et al., 2006). In our experiments, C57BL/6J mice that are homozygous for the *Nnt* mutation (Figure S5A) showed increased fur pigmentation compared with C57BL6/NJ control (wild-type *Nnt*) mice (Figure 4A, left panel). Quantification of pheomelanin and eumelanin levels in mouse hair by HPLC shows higher eumelanin, but not pheomelanin, in C57BL/6J mice compared with C57BL/6NJ mice (Figure 4A).

Next, a zebrafish (*Danio rerio*) model that selectively overexpresses NNT in melanocytes was engineered. Similar to humans and mice, zebrafish melanocytes originate from the neural crest, and the pathways leading to melanocyte differentiation and pigment production are conserved. Many human pigmentation genes and disorders have been modeled successfully in zebrafish, highlighting the striking similarity between zebrafish and human melanocytes. Unlike humans, zebrafish have xanthophore and iridophore pigmentation cells, but in this manuscript we restrict our studies to melanocytes (van Rooijen et al., 2017). Five days after NNT overexpression, a decrease in intramelanocytic pigmentation was observed in NNT-overexpressing zebrafish compared with empty-plasmid zebrafish embryos (Figure 4B). This observation was confirmed by pixel-based brightness quantification analysis. Deletion of *nnt* using CRISPR-Cas9 (Figure S5B) resulted in darkened melanocytes (Figure 4C). Similar to genetic deletion of *nnt*, treatment of zebrafish embryos for 24 h with chemical NNT inhibitors (DCC and 2,3BD), resulted in significant darkening (Figure 4D). However, subsequent treatment of NNT-overexpressing fish with 2,3BD prevented the NNT overexpression [OE]-induced decrease in melanocytic pigmentation (Figure S5C). This finding is in line with previous publications confirming an inhib-

itory role 2,3BD and DCC on NNT enzyme activity (Phelps and Hatefi, 1981; Moody and Reid, 1983). Next we examined the status of NNT in human hyperpigmentation disorders, including postinflammatory hyperpigmentation (PIH) and lentigo. Skin biopsies of nine Asian individuals were co-stained for NNT and 4',6-diamidino-2-phenylindole (DAPI) immunofluorescence. NNT intensity was normalized to the sample's DAPI intensity and cell count. Epidermal and upper dermal skin were investigated. In line with the Human Protein Atlas, NNT is expressed in different epidermal cells, including keratinocytes, fibroblasts, and melanocytes (Uhlén et al., 2015), moderate levels of NNT expression (red) were detected throughout the epidermis and upper dermis (Figure 4E, left panels). Although non-inflammatory skin disorders, such as ABNOM (acquired bilateral nevus of Ota-like macules, also known as Hori's nevus), displayed NNT expression levels similar to those of healthy skin (data not shown), skin of individuals with inflammation-induced disorders displayed decreased NNT expression levels. Disorders where intrinsic inflammation was present, such as PIH, or where extrinsic inflammation was present, such as UV-induced lentigo, NNT expression was significantly lower compared with healthy skin (Figure 4E, center and right panels). Interestingly, this trend was enhanced in areas of hyperpigmentation (Figure S5D).

Thus, NNT levels appear to be associated with murine and zebrafish pigmentation as well as human disorders of hyperpigmentation.

Statistical associations between genetic variants of NNT and human skin pigmentation variation in diverse population cohorts

Genetic associations

To investigate whether NNT plays a role in normal skin pigmentation variation in humans, we examined associations between pigmentation and genetic variants within the ~1.1-Mb *NNT* gene region. A meta-analysis was performed to combine *p* values from genome-wide association studies (GWASs) conducted in 4 diverse population cohorts with a total of 462,885 individuals: two Western European cohorts (Rotterdam Study [Jacobs et al., 2015] and UK Biobank [Hysi et al., 2018; Loh et al., 2018]), a multi-ethnic Latin American cohort (CANDELA; Adhikari et al., 2019), and a multi-ethnic cohort from eastern and southern Africa (Crawford et al., 2017). In these studies, skin pigmentation was measured quantitatively by reflectometry or by an ordinal system (STAR Methods). UK Biobank summary statistics were also available for ease of skin tanning (sunburn) and use of sun protection.

(C) Zebrafish with the *nnt* gene edited using CRISPR-Cas9 (NNT KO) display increased pigmentation after 4 days. A representative image is displayed. Results of mean melanocytic brightness, quantified by pixel-based analysis, are shown in the graph on the right. Control (*n* = 42 fish, 120 melanocytes), NNT KO (*n* = 50 fish, 96 melanocytes).

(D) Zebrafish treated for 24 h with 100 μ M 2,3BD or 50 μ M DCC display increased darkening after 4 days. A representative image is displayed. Results of mean melanocytic brightness, quantified by pixel-based analysis, are shown in the graph on the right. DMSO (*n* = 21 fish, 97 melanocytes), 2,3BD (*n* = 20 fish, 59 melanocytes), DCC (*n* = 18 fish, 57 melanocytes), analyzed by ordinary one-way ANOVA with Dunnett's post-test.

(E) Left panel: human skin specimens from Asian individuals with lentigo or PIH were compared with normal skin after staining for NNT, DAPI, and Fontana-Masson. Representative images of at least 3 samples are displayed (E, epidermis; D, dermis). The graph shows NNT signal intensities normalized to absolute cell numbers (DAPI); *n* = 3, analyzed by ordinary one-way ANOVA with Dunnett's post-test.

All data are expressed as mean \pm SEM; **p* < 0.05, ***p* < 0.01, ****p* < 0.001, *****p* < 0.0001.

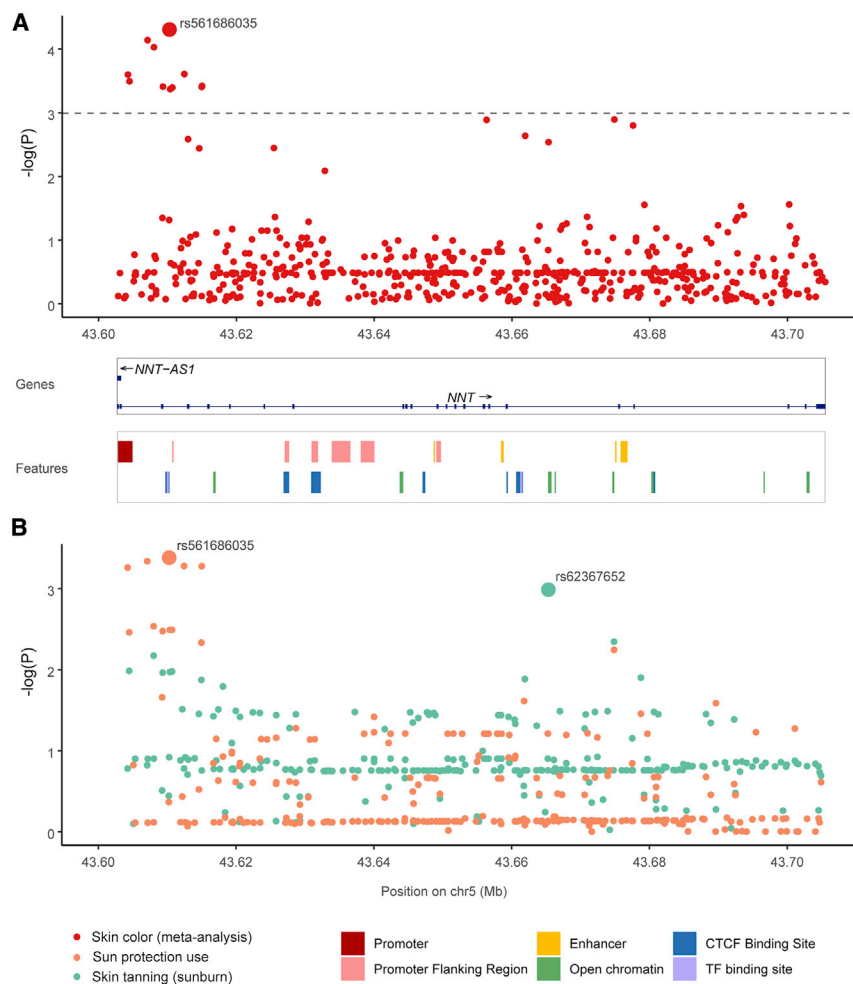


Figure 5. Association results for SNPs in the *NNT* gene with skin color in multiple cohorts

(A) p values of SNPs from a meta-analysis of skin color (red), combining association results from 4 worldwide cohorts across 462,885 individuals. For each of the 332 SNPs, its location in the *NNT* gene is shown on the x axis, and the negative logarithm of the p value is shown on the y axis. The SNP with the strongest association, rs561686035, is labeled. The adjusted significance threshold is shown with a dashed line. The *NNT* gene track and a track of regulatory regions obtained from the Ensembl genome browser are shown below.

(B) p values of SNPs from the UK Biobank for sun protection use (orange) and ease of skin tanning (sunburn) (green). For each SNP, its genomic location is shown on the x axis, and the negative logarithm of the p value is shown on the y axis. The SNPs with the strongest association for each trait, rs561686035 for sun protection use and rs62367652 for skin tanning, are labeled.

332 variants were available in the combined dataset; using a p value significance threshold of 1.01×10^{-3} (adjusted for multiple testing; STAR Methods), 11 variants were significantly associated with skin pigmentation in the meta-analysis (Figure 5A; Table S1). The variants were present in all worldwide populations, with the alternative alleles having the highest frequency in Africans (Table S1; Figure 6A) and being associated with darker skin color. The strongest association ($p = 4.94 \times 10^{-5}$) was observed for an intronic variant, rs561686035.

It was also the strongest associated variant for sun protection use in the UK Biobank cohort ($p = 4.15 \times 10^{-4}$; Figure 5B), with the minor allele being associated with increased use. The UK Biobank cohort also showed a significant association with ease of skin tanning (sunburn), with the lowest p value being 1×10^{-3} for the intronic SNP rs62367652 and the minor allele being associated with increased tanning (Figures 5B and S6B).

In silico expression analysis of *NNT* variants

All 11 variants that were significant in the meta-analysis of pigmentation are in linkage disequilibrium (LD) ($r^2 > 0.7$), and they span an 11-kb region at the beginning of the *NNT* gene overlapping its promoter (ENSR00000180214) (Figure 5A), which shows regulatory activity in melanocytes and keratinocytes (ac-

ording to the Ensembl database; Table S1). Furthermore, several of these variants are highly significant eQTLs (expression quantitative trait loci) for the *NNT* gene in sun-exposed and unexposed skin tissue (according to the genotype-tissue expression project [GTEx] database; Table S1). For these variants, the alternative alleles correlated with darker skin color and had negative effect sizes as eQTLs for *NNT* expression (Table S1), indicating lower levels of expression of the *NNT* transcript.

Subsequently, we sought to understand the direction of effect of the *NNT* genetic variants on these traits and on

expression of *NNT*. We calculated the correlation between the GWAS effect sizes of the alternative allele of each genetic variant within the *NNT* region with their effect sizes as eQTLs on expression of the *NNT* transcript according to GTEx in the two skin tissues (STAR Methods). The results are consistent with the direction of association between *NNT* transcript expression and skin color (especially in sun-unexposed skin tissue, where the effect of external factors such as sunlight is less prominent) and sun protection use (especially in sun-exposed skin tissue) as well as sunburn (especially in sun-exposed skin tissue).

Therefore, several intronic SNPs within the *NNT* genomic region were associated with skin pigmentation, tanning, and sun protection use in 4 diverse cohorts including 462,885 individuals. Using eQTL expression data for *NNT*, we observed that lower expression of the *NNT* transcript in skin tissues correlates with darker skin color and, consequently, less sunburn and less sun protection use.

Conditioning on known pigmentation SNPs

Because *MC1R* is a major determinant of pigmentation, with known genetic variants associated with lighter skin color, red

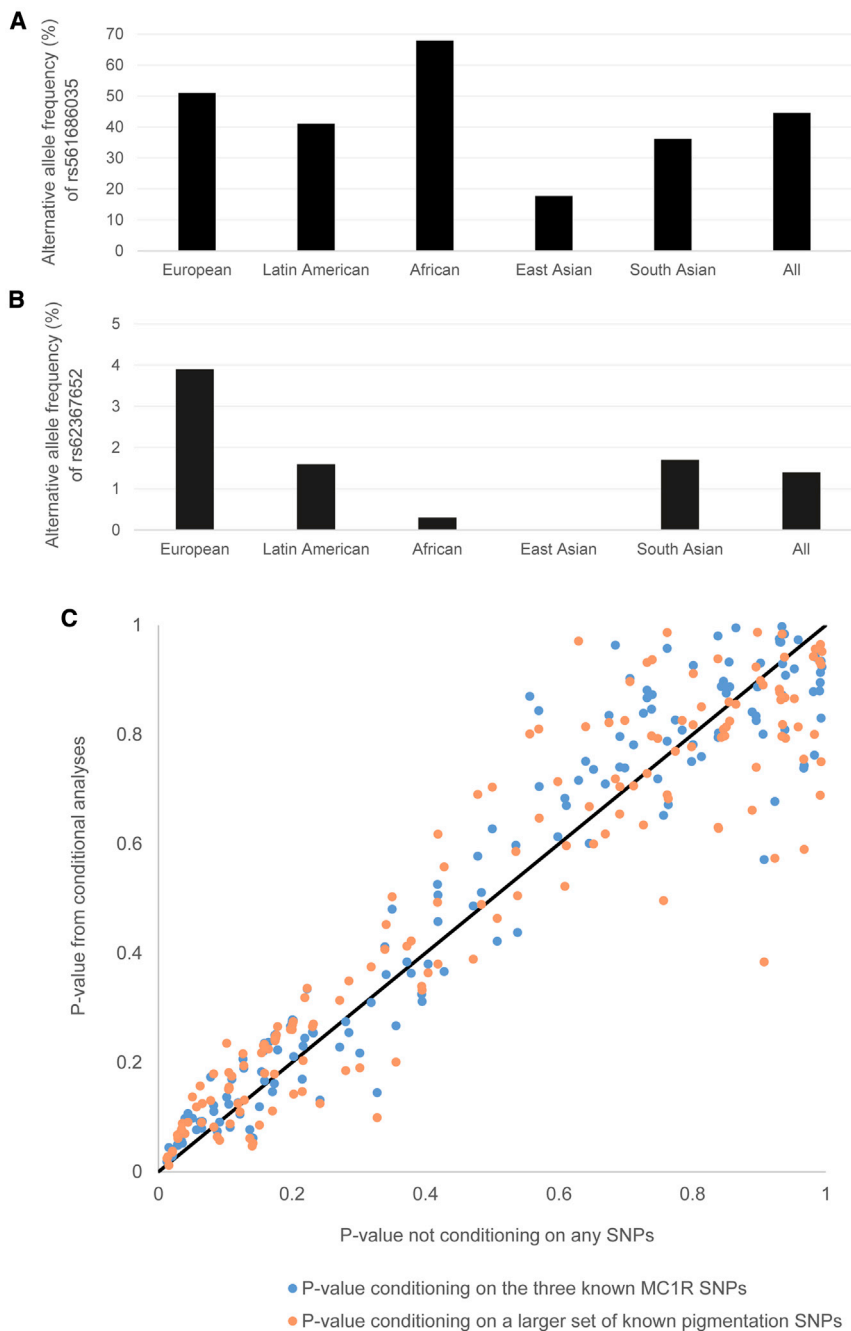


Figure 6. Association results and properties of SNPs from various human genetic association analyses

(A and B) Allele frequencies for SNPs in the NNT gene showing the most significant associations.

(A) Alternative allele frequencies of rs561686035 in various worldwide continental populations, obtained from 1000 Genomes Phase 3. This SNP showed the strongest association in the meta-analysis of skin color and for sun protection use.

(B) Alternative allele frequencies of rs62367652 in various worldwide continental populations, obtained from 1000 Genomes Phase 3. This SNP showed the strongest association for ease of skin tanning (sunburn).

(C) Association results for SNPs in the NNT gene with or without conditioning on known pigmentation loci. p values of SNPs from the Rotterdam Study are shown in this scatterplot. The x axis represents p values of SNPs from the standard GWAS analysis of skin pigmentation (not conditioned on any other SNP). p values from two conditional analyses are plotted on the y axis: blue, p values conditioning on the three known MC1R SNPs; orange, p value conditioning on a larger set of known pigmentation SNPs. A diagonal line in black is shown for reference.

DISCUSSION

This study addresses the question of how redox metabolism interplays with skin pigmentation. It identifies (1) the existence of a distinct redox-dependent, UV- and MITF-independent skin pigmentation mechanism; (2) a role of the mitochondrial redox-regulating enzyme NNT in altering pigmentation by regulating tyrosinase protein stability and melanosome maturation via a redox-dependent mechanism; and (3) a class of topical NNT inhibitors that yield skin darkening (Martin et al., 2017).

SLC24A5 was the first gene to be identified as associated with light skin color in Europeans (Lamason et al., 2005). GWAS in non-Europeans (Arjinpathana and Asawanonda, 2012; Crawford et al., 2017; Hysi et al., 2018; Lin et al., 2018; Martin

et al., 2017) emphasized the complex nature of human skin pigmentation. In addition to certain key regulators such as TYR and MITF, many other genes may affect skin pigmentation and an individual's skin color. It is thus plausible that factors involved in redox metabolism, such as NNT, may be responsive to environmental changes such as UV exposure or inflammation. Increasing eumelanin levels as a response to ROS-inducing events might have been beneficial during evolution by maintaining cutaneous redox equilibrium. An interplay between oxidative stress and skin pigmentation has been suspected (Arjinpathana

hair, and freckles in European populations (Quillen et al., 2019), we checked whether MC1R can be a confounder in the observed association of NNT with skin pigmentation. In the Western European cohort of the Rotterdam Study, conditioning on the three known MC1R SNPs in the GWAS did not significantly alter the p values of the NNT variants ($p = 0.869$; Figure 6B). Conditioning on a larger set of known pigmentation variants (STAR Methods) in the GWAS does not significantly alter the p values of the NNT variants ($p = 0.191$; Figure 6C) either.

and Asawanonda, 2012), but the exact mechanism and ways to potentially target this pathway are incompletely elucidated.

From a clinical perspective, our findings are relevant because of the prevalence of pigmentary disorders, which are among the most common reasons for dermatological consultations (Cestari et al., 2014). In addition, lightly pigmented individuals have increased risk of melanoma, a life-threatening disease.

As shown previously (D'Orazio et al., 2006; Mujahid et al., 2017), skin pigmentation, and especially high eumelanin levels, can protect human skin from UVB-induced CPD formation. Most probably, this effect relates to eumelanin-mediated absorbance of UV light and a buffering function of eumelanin toward oxidative stress radicals. Different approaches for increasing pigmentation have been tried so far, including topical use of the cAMP agonist forskolin (D'Orazio et al., 2006), which worked well in mice but does not sufficiently penetrate human skin. Afa-melanotide, an α -MSH analog, has been used for treating erythropoietic protoporphyria by producing hyperpigmentation that is able to protect skin against UV light-induced photosensitivity (Langendonk et al., 2015). Topical administration of SIK inhibitors preclinically also induced pigmentation (Horike et al., 2010; Mujahid et al., 2017). Because MITF is a transcription factor involved in numerous melanocyte functions, transiently targeting pigmentation via NNT inhibition is a distinct and potentially complementary approach that might have applications in contexts such as pigmentation disorders and skin cancer prevention.

In this report, we present evidence of the existence of a redox-dependent skin pigmentation pathway. In contrast to the established classic UVB-cAMP-MITF-dependent tanning pathway, this mechanism is independent of UV irradiation, MITF, and MITF signaling effects. Instead, a distinct pigmentation mechanism dependent on ROS is described, demonstrating how oxidative stress affects pigmentation in cells of melanocytic origin by modifying GSH, NADPH, increasing tyrosinase protein stability, tyrosinase-related proteins, and melanosome maturation. Evaluating the interplay between other pigmentation mechanisms, such as immediate and persistent pigment darkening, as well as understanding the safety, penetration, and efficacy of topical NNT modifiers may be worthy of study in future clinical settings.

Limitations of the study

In this proof-of-principle study, the effect of NNT on pigmentation has been shown. However, there are several limitations:

- (1) Although this study used previously identified NNT-inhibiting compounds, further research is needed to identify more specific compounds for modulating NNT enzyme activity. We believe caution is warranted when modulating cutaneous redox biology and skin pigmentation, requiring careful attention before human application.
- (2) We used the NntC57BL/6J mouse model, which is homozygous for the NntC57BL/6J mutation and lack a stretch of 17,814 bp between exons 6 and 12, resulting in a lack of mature NNT protein. Because this mutation also affects the function of other proteins, use of this model alone cannot confirm NNT's role in pigmentation.
- (3) The statistical association analyses identify a correlation between SNPs within NNT and human pigmentation vari-

ation. Although some of the associated SNPs are located within the promoter region of the NNT gene and are eQTLs for NNT expression, further biological experiments are needed to confirm causality.

- (4) Although zebrafish melanocyte function and melanin biosynthesis are similar to humans because many genes are shared, the contribution of other fish-specific cell types to melanocyte biology is incompletely understood. The MiniCoopR rescue system employed in this study overexpresses human NNT potentially at above physiological levels. This seems to cause slight toxicity to melanocytes, which resulted in lower melanocyte rescue. Additionally, because of technical variability in single-cell injection efficiency, variations in the number and location of melanocytes per fish were observed.

STAR★METHODS

Detailed methods are provided in the online version of this paper and include the following:

- **KEY RESOURCES TABLE**
- **RESOURCE AVAILABILITY**
 - Lead contact
 - Materials availability
 - Data and code availability
- **EXPERIMENTAL MODEL AND SUBJECT DETAILS**
 - Ethics Statement
 - Mice
 - Zebrafish
 - Human skin explants
 - Cell lines
- **METHOD DETAILS**
 - siRNA transfection
 - Plasmid overexpression
 - Lentivirus generation and infection
 - *In vitro* culture with NNT inhibitors
 - Immunoblotting
 - RNA purification and quantitative RT-PCR
 - Cycloheximide chase assay
 - Melanin quantification
 - Eumelanin and pheomelanin analysis
 - Skin colorimeter measurements
 - Determination of intracellular cAMP content
 - Cell viability assay
 - Glutathione measurements
 - Determination of NADPH/NADP ratio
 - Luciferase reporter assay
 - Histology and Immunofluorescence
 - Detection of cellular reactive oxygen species (ROS)
 - Transmission electron microscopy
 - Melanosomes-mitochondria distance measurements
 - Melanosome stage quantification
 - Tyrosinase activity assay
 - Human genetic association studies
 - Ethics Approval
 - A. The Rotterdam Study

- B. The CANDELA cohort
- C. The East & South African cohort
- D. The UK Biobank cohort
- Meta-analysis of the cohorts
- Multiple testing adjustment
- GWAS conditional on known pigmentation variants
- Correlation between trait effect sizes and eQTL expression data
- **QUANTIFICATION AND STATISTICAL ANALYSIS**
 - Statistical analysis

SUPPLEMENTAL INFORMATION

Supplemental information can be found online at <https://doi.org/10.1016/j.cell.2021.06.022>.

ACKNOWLEDGMENTS

We thank C. Thomas Powell and Robert Liu for help with statistical analysis and editing, Diane Capen for help with electron microscopy-related questions, Sharon Germana for administrative help, Paolo Gameiro for providing plasmid constructs, Pawel Pelczar for his efforts to generate transgenic mice, and Ruth Halaban, Micky Marks, Doug Richardson, Desmond Tobin, Rizwan Haq, Pere Puigserver, Alfred Goldberg, Lajos Kemeny senior, and Steven Gygi for helpful discussions. E.R. gratefully acknowledges support from the Mildred Scheel Grant of the German Cancer Society and the Filling the Gap Grant of the University of Zurich, Switzerland. D.E.F. gratefully acknowledges support from NIH grants 5P01-CA163222, 5R01CA222871, 5R01AR043369, and 5R01AR072304 and the Dr. Miriam and Sheldon Adelson Medical Research Foundation. S.T. is funded by NIH grants R01AR076241 and R35 GM134957-01. This work was conducted with support from Harvard Catalyst | The Harvard Clinical and Translational Science Center (National Center for Advancing Translational Sciences, National Institutes of Health award UL1TR002541) and financial contributions from Harvard University and its affiliated academic healthcare centers. The content is solely the responsibility of the authors and does not necessarily represent the official views of Harvard Catalyst, Harvard University and its affiliated academic healthcare centers, or the National Institutes of Health. P.P.N. was supported by the Swiss National Science Foundation (SNSF). Early Postdoctoral Mobility Fellowship CRSII3_154461 and Postdoctoral Mobility Fellowship P400PB_199252. B.P.K. was supported by NCI R00 CA218870 and NHLBI P01 HL142494. K.A. was supported by the Santander Research and Scholarship Award, and Bogue Fellowship from University College London. A.R.L. was supported by the Leverhulme Trust (F/07 134/DF), BBSRC (BB/1021213/1), the Excellence Initiative of Aix-Marseille University - A*MIDEX (a French “Investissements d’Avenir” program, 2RUJZLRE/RHRE/ID18HRU201 and 20-07874), the National Natural Science Foundation of China (31771393), the Scientific and Technology Committee of Shanghai Municipality (18490750300), the Ministry of Science and Technology of China (2020YFE0201600), the Shanghai Municipal Science and Technology Major Project (2017SHZDZX01), and the 111 Project (B13016). G.B. was supported by the Universidad de Antioquia (CODI sostenibilidad de grupos 2013–2014 and MASO 2013–2014). L.V.K. is a recipient of the János Bolyai Research Scholarship of the Hungarian Academy of Sciences. The Rotterdam Study is funded by Erasmus Medical Center and Erasmus University Rotterdam (the Netherlands); the Netherlands Organization for the Health Research and Development (ZonMw); the Research Institute for Diseases in the Elderly; the Ministry of Education, Culture and Science; the Ministry for Health, Welfare and Sports; the European Commission (DG XII); and the Municipality of Rotterdam. The Microscopy Core of the MGH Program in Membrane Biology is partially supported by Inflammatory Bowel Disease Center grant DK043351 and Boston Area Diabetes Endocrinology Research Center grant DK057521.

AUTHOR CONTRIBUTIONS

E.R. and D.E.F. conceived the project. E.R., J.A., I.R., and D.E.F. designed and discussed the experiments. E.R., I.R., J.A., Y.S., S.K., A.K., V.I., J.Z., H.W.,

A.L., M.V.S., K.W., B.P.K., K.A.C., and S.I. performed *in vitro* studies. J.A., I.R., and J.H.L. performed histological analyses. A.C., H.R.N., and L.Z. performed zebrafish experiments. E.R., V.I., J.A., and J.A.L. performed mouse studies and prepared photographic images. K.A., L.M.P., S.F., R.G.-J., M.-C.B., S.C.-Q., V.A.-A., C.G., G.P., G.B., F.R., T.N., S.T., and A.R.-L. performed human genetic association studies. C.M.L., N.M., J.A.L., C.H.W., S.O., J.Z., N.N., Q.Y.W., H.W., C.L.E., M.V.S., P.P.N., K.I., I.N., L.H.C., A.A.N., J.J.H., C.B., and T.R. assisted with the experimental design and data interpretation. E.R., J.A., I.R., K.A., L.M.P., and S.K. prepared figures. E.R., I.R., K.A., J.A., and D.E.F. wrote the manuscript. All authors discussed the results and commented on the manuscript.

DECLARATION OF INTERESTS

D.E.F. and E.R. have a patent filed on “Methods and compositions for enhancing skin pigmentation” (publication number WO/2016/077817, May 19, 2016.). D.E.F. has a financial interest in Soltego, Inc., a company developing SIK inhibitors for topical skin darkening treatments that might be used for a broad set of human applications. D.E.F.’s interests were reviewed and are managed by Massachusetts General Hospital and Partners HealthCare in accordance with their conflict-of-interest policies. B.P.K. is an inventor on patents and patent applications filed by Mass General Brigham that describe genome engineering technologies. B.P.K. consults for Avestas Inc., ElevateBio, and EcoR1 capital and is an advisor to Acrogen Biosciences. Q.Y.W. is a shareholder in Mymiel Skincare. L.I.Z. is a founder and stockholder of Fate Therapeutics, CAMP4 Therapeutics, Amagma Therapeutics, and Scholar Rock. He is a consultant for Celularity and Cellarity. H.W. is an employee and shareholder of Johnson and Johnson.

Received: September 21, 2020

Revised: March 9, 2021

Accepted: June 15, 2021

Published: July 6, 2021

REFERENCES

- Abecasis, G.R., Auton, A., Brooks, L.D., DePristo, M.A., Durbin, R.M., Handsaker, R.E., Kang, H.M., Marth, G.T., and McVean, G.A.; 1000 Genomes Project Consortium (2012). An integrated map of genetic variation from 1,092 human genomes. *Nature* 491, 56–65.
- Ablain, J., Durand, E.M., Yang, S., Zhou, Y., and Zon, L.I. (2015). A CRISPR/Cas9 vector system for tissue-specific gene disruption in zebrafish. *Dev. Cell* 32, 756–764.
- Adhikari, K., Mendoza-Revilla, J., Sohail, A., Fuentes-Guajardo, M., Lampert, J., Chacón-Duque, J.C., Hurtado, M., Villegas, V., Granja, V., Acuña-Alonso, V., et al. (2019). A GWAS in Latin Americans highlights the convergent evolution of lighter skin pigmentation in Eurasia. *Nat. Commun.* 10, 358.
- Allouche, J., Bellon, N., Saidani, M., Stanchina-Chatrousse, L., Masson, Y., Patwardhan, A., Gilles-Marsens, F., Delevoye, C., Domingues, S., Nissan, X., et al. (2015). In vitro modeling of hyperpigmentation associated to neurofibromatosis type 1 using melanocytes derived from human embryonic stem cells. *Proc. Natl. Acad. Sci. USA* 112, 9034–9039.
- Arjinpethana, N., and Asawanonda, P. (2012). Glutathione as an oral whitening agent: a randomized, double-blind, placebo-controlled study. *J. Dermatolog. Treat.* 23, 97–102.
- Bae, S., Park, J., and Kim, J.S. (2014). Cas-OFFinder: a fast and versatile algorithm that searches for potential off-target sites of Cas9 RNA-guided endonucleases. *Bioinformatics* 30, 1473–1475.
- Barth, S., Glick, D., and Macleod, K.F. (2010). Autophagy: assays and artifacts. *J. Pathol.* 221, 117–124.
- Bellei, B., Maresca, V., Flori, E., Pitisci, A., Larue, L., and Picardo, M. (2010). p38 regulates pigmentation via proteasomal degradation of tyrosinase. *J. Biol. Chem.* 285, 7288–7299.
- Benjamini, Y., and Cohen, R. (2017). Weighted false discovery rate controlling procedures for clinical trials. *Biostatistics* 18, 91–104.

- Bennett, D.C., Cooper, P.J., and Hart, I.R. (1987). A line of non-tumorigenic mouse melanocytes, syngeneic with the B16 melanoma and requiring a tumour promoter for growth. *Int. J. Cancer* 39, 414–418.
- Berger, M.F., Hodis, E., Heffernan, T.P., Deribe, Y.L., Lawrence, M.S., Protopopov, A., Ivanova, E., Watson, I.R., Nickerson, E., Ghosh, P., et al. (2012). Melanoma genome sequencing reveals frequent PREX2 mutations. *Nature* 485, 502–506.
- Ceol, C.J., Houvras, Y., Jane-Valbuena, J., Bilodeau, S., Orlando, D.A., Battisti, V., Fritsch, L., Lin, W.M., Hollmann, T.J., Ferré, F., et al. (2011). The histone methyltransferase SETDB1 is recurrently amplified in melanoma and accelerates its onset. *Nature* 471, 513–517.
- Cestari, T.F., Dantas, L.P., and Boza, J.C. (2014). Acquired hyperpigmentation. *An. Bras. Dermatol.* 89, 11–25.
- Clement, K., Rees, H., Canver, M.C., Gehrke, J.M., Farouni, R., Hsu, J.Y., Cole, M.A., Liu, D.R., Joung, J.K., Bauer, D.E., and Pinello, L. (2019). CRISPResso2 provides accurate and rapid genome editing sequence analysis. *Nat. Biotechnol.* 37, 224–226.
- Crawford, N.G., Kelly, D.E., Hansen, M.E.B., Beltrame, M.H., Fan, S., Bowman, S.L., Jewett, E., Ranciaro, A., Thompson, S., Lo, Y., et al.; NISC Comparative Sequencing Program (2017). Loci associated with skin pigmentation identified in African populations. *Science* 358, eaan8433.
- d'Ischia, M., Wakamatsu, K., Napolitano, A., Briganti, S., Garcia-Borron, J.C., Kovacs, D., Meredith, P., Pezzella, A., Picardo, M., Sarna, T., et al. (2013). Melanins and melanogenesis: methods, standards, protocols. *Pigment Cell Melanoma Res.* 26, 616–633.
- D'Orazio, J.A., Nobuhisa, T., Cui, R., Arya, M., Spry, M., Wakamatsu, K., Igras, V., Kunisada, T., Granter, S.R., Nishimura, E.K., et al. (2006). Topical drug rescue strategy and skin protection based on the role of Mc1r in UV-induced tanning. *Nature* 443, 340–344.
- Daniele, T., Hurbain, I., Vago, R., Casari, G., Raposo, G., Tacchetti, C., and Schiaffino, M.V. (2014). Mitochondria and melanosomes establish physical contacts modulated by Mfn2 and involved in organelle biogenesis. *Curr. Biol.* 24, 393–403.
- Del Bino, S., Ito, S., Sok, J., Nakanishi, Y., Bastien, P., Wakamatsu, K., and Bernerd, F. (2015). Chemical analysis of constitutive pigmentation of human epidermis reveals constant eumelanin to pheomelanin ratio. *Pigment Cell Melanoma Res.* 28, 707–717.
- Earle, S.R., and Fisher, R.R. (1980). A direct demonstration of proton translocation coupled to transhydrogenation in reconstituted vesicles. *J. Biol. Chem.* 255, 827–830.
- Filadi, R., Penden, D., and Pizzo, P. (2018). Mitofusin 2: from functions to disease. *Cell Death Dis.* 9, 330.
- Ho, H., and Ganesan, A.K. (2011). The pleiotropic roles of autophagy regulators in melanogenesis. *Pigment Cell Melanoma Res.* 24, 595–604.
- Hofman, A., Brusselle, G.G., Darwish Murad, S., van Duijn, C.M., Franco, O.H., Goedegebure, A., Ikram, M.A., Klaver, C.C., Nijsten, T.E., Peeters, R.P., et al. (2015). The Rotterdam Study: 2016 objectives and design update. *Eur. J. Epidemiol.* 30, 661–708.
- Horike, N., Kumagai, A., Shimono, Y., Onishi, T., Itoh, Y., Sasaki, T., Kitagawa, K., Hatano, O., Takagi, H., Susumu, T., et al. (2010). Downregulation of SIK2 expression promotes the melanogenic program in mice. *Pigment Cell Melanoma Res.* 23, 809–819.
- Huang, T.T., Naeemuddin, M., Elchuri, S., Yamaguchi, M., Kozy, H.M., Carlson, E.J., and Epstein, C.J. (2006). Genetic modifiers of the phenotype of mice deficient in mitochondrial superoxide dismutase. *Hum. Mol. Genet.* 15, 1187–1194.
- Hysi, P.G., Valdes, A.M., Liu, F., Furlotte, N.A., Evans, D.M., Bataille, V., Visconti, A., Hemani, G., McMahon, G., Ring, S.M., et al.; International Visible Trait Genetics Consortium (2018). Genome-wide association meta-analysis of individuals of European ancestry identifies new loci explaining a substantial fraction of hair color variation and heritability. *Nat. Genet.* 50, 652–656.
- Ikram, M.A., Brusselle, G.G.O., Murad, S.D., van Duijn, C.M., Franco, O.H., Goedegebure, A., Klaver, C.C.W., Nijsten, T.E.C., Peeters, R.P., Stricker, B.H., et al. (2017). The Rotterdam Study: 2018 update on objectives, design and main results. *Eur. J. Epidemiol.* 32, 807–850.
- Iozumi, K., Hoganson, G.E., Pennella, R., Everett, M.A., and Fuller, B.B. (1993). Role of tyrosinase as the determinant of pigmentation in cultured human melanocytes. *J. Invest. Dermatol.* 100, 806–811.
- Ito, S.; IFPCS (2003). The IFPCS presidential lecture: a chemist's view of melanogenesis. *Pigment Cell Res.* 16, 230–236.
- Ito, S., Nakanishi, Y., Valenzuela, R.K., Brilliant, M.H., Kolbe, L., and Wakamatsu, K. (2011). Usefulness of alkaline hydrogen peroxide oxidation to analyze eumelanin and pheomelanin in various tissue samples: application to chemical analysis of human hair melanins. *Pigment Cell Melanoma Res.* 24, 605–613.
- Jablonski, N.G., and Chaplin, G. (2012). Human skin pigmentation, migration and disease susceptibility. *Philos. Trans. R. Soc. Lond. B Biol. Sci.* 367, 785–792.
- Jablonski, N.G., and Chaplin, G. (2017). The colours of humanity: the evolution of pigmentation in the human lineage. *Philos. Trans. R. Soc. Lond. B Biol. Sci.* 372, 20160349.
- Jacobs, L.C., Hamer, M.A., Verkouteren, J.A., Pardo, L.M., Liu, F., and Nijsten, T. (2015). Perceived skin colour seems a swift, valid and reliable measurement. *Br. J. Dermatol.* 173, 1084–1086.
- Jara, J.R., Aroca, P., Solano, F., Martinez, J.H., and Lozano, J.A. (1988). The role of sulfhydryl compounds in mammalian melanogenesis: the effect of cysteine and glutathione upon tyrosinase and the intermediates of the pathway. *Biochim. Biophys. Acta* 967, 296–303.
- Jaruga, P., and Dizdaroğlu, M. (2008). 8,5'-Cyclopurine-2'-deoxynucleosides in DNA: mechanisms of formation, measurement, repair and biological effects. *DNA Repair (Amst.)* 7, 1413–1425.
- Jiang, L., Zheng, Z., Qi, T., Kemper, K.E., Wray, N.R., Visscher, P.M., and Yang, J. (2019). A resource-efficient tool for mixed model association analysis of large-scale data. *Nat. Genet.* 51, 1749–1755.
- Khaled, M., Levy, C., and Fisher, D.E. (2010). Control of melanocyte differentiation by a MITF-PDE4D3 homeostatic circuit. *Genes Dev.* 24, 2276–2281.
- King, R., Weillbaeher, K.N., McGill, G., Cooley, E., Mihm, M., and Fisher, D.E. (1999). Microphthalmia transcription factor. A sensitive and specific melanocyte marker for MelanomaDiagnosis. *Am. J. Pathol.* 155, 731–738.
- Kleinstiver, B.P., Sousa, A.A., Walton, R.T., Tak, Y.E., Hsu, J.Y., Clement, K., Welch, M.M., Horng, J.E., Malagon-Lopez, J., Scarfò, I., et al. (2019). Engineered CRISPR-Cas12a variants with increased activities and improved targeting ranges for gene, epigenetic and base editing. *Nat. Biotechnol.* 37, 276–282.
- Labun, K., Montague, T.G., Krause, M., Torres Cleuren, Y.N., Tjeldnes, H., and Valen, E. (2019). CHOPCHOP v3: expanding the CRISPR web toolbox beyond genome editing. *Nucleic Acids Res.* 47 (W1), W171–W174.
- Lamason, R.L., Mohideen, M.A., Mest, J.R., Wong, A.C., Norton, H.L., Aros, M.C., Juryneć, M.J., Mao, X., Humphreville, V.R., Humbert, J.E., et al. (2005). SLC24A5, a putative cation exchanger, affects pigmentation in zebrafish and humans. *Science* 310, 1782–1786.
- Langendonk, J.G., Balwani, M., Anderson, K.E., Bonkovsky, H.L., Anstey, A.V., Bissell, D.M., Bloomer, J., Edwards, C., Neumann, N.J., Parker, C., et al. (2015). Afamelanotide for Erythropoietic Protoporphyrria. *N. Engl. J. Med.* 373, 48–59.
- Leboucher, G.P., Tsai, Y.C., Yang, M., Shaw, K.C., Zhou, M., Veenstra, T.D., Glickman, M.H., and Weissman, A.M. (2012). Stress-induced phosphorylation and proteasomal degradation of mitofusin 2 facilitates mitochondrial fragmentation and apoptosis. *Mol. Cell* 47, 547–557.
- Lin, M., Siford, R.L., Martin, A.R., Nakagome, S., Möller, M., Hoal, E.G., Bustamante, C.D., Gignoux, C.R., and Henn, B.M. (2018). Rapid evolution of a skin-lightening allele in southern African Khoesan. *Proc. Natl. Acad. Sci. USA* 115, 13324–13329.
- Lo, J.A., and Fisher, D.E. (2014). The melanoma revolution: from UV carcinogenesis to a new era in therapeutics. *Science* 346, 945–949.
- Loh, P.R., Kichaev, G., Gazal, S., Schoech, A.P., and Price, A.L. (2018). Mixed-model association for biobank-scale datasets. *Nat. Genet.* 50, 906–908.

- Martin, A.R., Lin, M., Granka, J.M., Myrick, J.W., Liu, X., Sockell, A., Atkinson, E.G., Weryly, C.J., Möller, M., Sandhu, M.S., et al. (2017). An Unexpectedly Complex Architecture for Skin Pigmentation in Africans. *Cell* 171, 1340–1353.e14.
- Mitra, D., Luo, X., Morgan, A., Wang, J., Hoang, M.P., Lo, J., Guerrero, C.R., Lennerz, J.K., Mihm, M.C., Wargo, J.A., et al. (2012). An ultraviolet-radiation-independent pathway to melanoma carcinogenesis in the red hair/fair skin background. *Nature* 491, 449–453.
- Moody, A.J., and Reid, R.A. (1983). Inhibition of nicotinamide nucleotide transhydrogenase in rat liver submitochondrial particles by dicyclohexylcarbodiimide and butanedione. *Biochem. J.* 209, 889–892.
- Moreno-Mateos, M.A., Vejnar, C.E., Beaudoin, J.D., Fernandez, J.P., Mis, E.K., Khokha, M.K., and Giraldez, A.J. (2015). CRISPRscan: designing highly efficient sgRNAs for CRISPR-Cas9 targeting in vivo. *Nat. Methods* 12, 982–988.
- Mujahid, N., Liang, Y., Murakami, R., Choi, H.G., Dobry, A.S., Wang, J., Suita, Y., Weng, Q.Y., Allouche, J., Kemeny, L.V., et al. (2017). A UV-Independent Topical Small-Molecule Approach for Melanin Production in Human Skin. *Cell Rep.* 19, 2177–2184.
- Park, S.B., Suh, D.H., and Youn, J.I. (1999). A long-term time course of colorimetric evaluation of ultraviolet light-induced skin reactions. *Clin. Exp. Dermatol.* 24, 315–320.
- Park, H.Y., Kosmadaki, M., Yaar, M., and Gilchrist, B.A. (2009). Cellular mechanisms regulating human melanogenesis. *Cell. Mol. Life Sci.* 66, 1493–1506.
- Paterson, E.K., Fielder, T.J., MacGregor, G.R., Ito, S., Wakamatsu, K., Gillen, D.L., Eby, V., Boissy, R.E., and Ganesan, A.K. (2015). Tyrosinase Depletion Prevents the Maturation of Melanosomes in the Mouse Hair Follicle. *PLoS ONE* 10, e0143702.
- Pathak, M.A., Riley, F.J., Fitzpatrick, T.B., and Curwen, W.L. (1962). Melanin formation in human skin induced by long-wave ultra-violet and visible light. *Nature* 193, 148–150.
- Phelps, D.C., and Hatefi, Y. (1981). Inhibition of the mitochondrial nicotinamide nucleotide transhydrogenase by dicyclohexylcarbodiimide and diethylpyrocarbonate. *J. Biol. Chem.* 256, 8217–8221.
- Premi, S., Wallisch, S., Mano, C.M., Weiner, A.B., Bacchiocchi, A., Wakamatsu, K., Bechara, E.J., Halaban, R., Douki, T., and Brash, D.E. (2015). Photochemistry. Chemiexcitation of melanin derivatives induces DNA photoproducts long after UV exposure. *Science* 347, 842–847.
- Purcell, S., Neale, B., Todd-Brown, K., Thomas, L., Ferreira, M.A., Bender, D., Maller, J., Sklar, P., de Bakker, P.I., Daly, M.J., and Sham, P.C. (2007). PLINK: a tool set for whole-genome association and population-based linkage analyses. *Am. J. Hum. Genet.* 81, 559–575.
- Quillen, E.E., Norton, H.L., Parra, E.J., Lona-Durazo, F., Ang, K.C., Illiescu, F.M., Pearson, L.N., Shriver, M.D., Lasiqi, T., Gokcumen, O., et al. (2019). Shades of complexity: New perspectives on the evolution and genetic architecture of human skin. *Am. J. Phys. Anthropol.* 168 (Suppl 67), 4–26.
- Raposo, G., and Marks, M.S. (2007). Melanosomes—dark organelles enlighten endosomal membrane transport. *Nat. Rev. Mol. Cell Biol.* 8, 786–797.
- Rendon, M.I., and Gaviria, J.I. (2005). Review of skin-lightening agents. *Dermatologic Surgery* 31, 886–889, discussion 889.
- Rigler, M.W., and Longo, W.E. (2010). Emission of diacetyl (2,3 butanedione) from natural butter, microwave popcorn butter flavor powder, paste, and liquid products. *Int. J. Occup. Environ. Health* 16, 291–302.
- Rohland, N., and Reich, D. (2012). Cost-effective, high-throughput DNA sequencing libraries for multiplexed target capture. *Genome Res.* 22, 939–946.
- Ronchi, J.A., Figueira, T.R., Ravagnani, F.G., Oliveira, H.C., Vercesi, A.E., and Castilho, R.F. (2013). A spontaneous mutation in the nicotinamide nucleotide transhydrogenase gene of C57BL/6J mice results in mitochondrial redox abnormalities. *Free Radic. Biol. Med.* 63, 446–456.
- Rydström, J. (1972). Site-specific inhibitors of mitochondrial nicotinamide nucleotide transhydrogenase. *Eur. J. Biochem.* 31, 496–504.
- Rydström, J., Teixeira da Cruz, A., and Ernster, L. (1970). Factors governing the steady state of the mitochondrial nicotinamide nucleotide transhydrogenase system. *Biochem. J.* 116, 12P–13P.
- Sancak, Y., Peterson, T.R., Shaul, Y.D., Lindquist, R.A., Thoreen, C.C., Bar-Peled, L., and Sabatini, D.M. (2008). The Rag GTPases bind raptor and mediate amino acid signaling to mTORC1. *Science* 320, 1496–1501.
- Schindelin, J., Arganda-Carreras, I., Frise, E., Kaynig, V., Longair, M., Pietzsch, T., Preibisch, S., Rueden, C., Saalfeld, S., Schmid, B., et al. (2012). Fiji: an open-source platform for biological-image analysis. *Nat. Methods* 9, 676–682.
- Sebastián, D., Soriano, E., Segalés, J., Irazoki, A., Ruiz-Bonilla, V., Sala, D., Planet, E., Berenguer-Llergo, A., Muñoz, J.P., Sánchez-Feutrie, M., et al. (2016). Mfn2 deficiency links age-related sarcopenia and impaired autophagy to activation of an adaptive mitophagy pathway. *EMBO J.* 35, 1677–1693.
- Sheeran, F.L., Rydström, J., Shakhparonov, M.I., Pestov, N.B., and Pepe, S. (2010). Diminished NADPH transhydrogenase activity and mitochondrial redox regulation in human failing myocardium. *Biochim. Biophys. Acta* 1797, 1138–1148.
- Steingrímsson, E., Copeland, N.G., and Jenkins, N.A. (2004). Melanocytes and the microphthalmia transcription factor network. *Annu. Rev. Genet.* 38, 365–411.
- Toye, A.A., Lippiat, J.D., Proks, P., Shimomura, K., Bentley, L., Hugill, A., Mijat, V., Goldsworthy, M., Moir, L., Haynes, A., et al. (2005). A genetic and physiological study of impaired glucose homeostasis control in C57BL/6J mice. *Diabetologia* 48, 675–686.
- Truett, G.E., Heeger, P., Mynatt, R.L., Truett, A.A., Walker, J.A., and Warman, M.L. (2000). Preparation of PCR-quality mouse genomic DNA with hot sodium hydroxide and tris (HotSHOT). *Biotechniques* 29, 52–54. <https://doi.org/10.2144/00291bm09>.
- Ugwu, S.O., Blanchard, J., Dorr, R.T., Levine, N., Brooks, C., Hadley, M.E., Aickin, M., and Hruby, V.J. (1997). Skin pigmentation and pharmacokinetics of melanotan-I in humans. *Biopharm. Drug Dispos.* 18, 259–269.
- Uhlén, M., Fagerberg, L., Hallström, B.M., Lindskog, C., Oksvold, P., Mardinoglu, A., Sivertsson, Å., Kampf, C., Sjöstedt, E., Asplund, A., et al. (2015). Proteomics. Tissue-based map of the human proteome. *Science* 347, 1260419.
- van Rooijen, E., Fazio, M., and Zon, L.I. (2017). From fish bowl to bedside: The power of zebrafish to unravel melanoma pathogenesis and discover new therapeutics. *Pigment Cell Melanoma Res.* 30, 402–412.
- Vazquez, F., Lim, J.H., Chim, H., Bhalla, K., Girnun, G., Pierce, K., Clish, C.B., Granter, S.R., Widlund, H.R., Spiegelman, B.M., and Puigserver, P. (2013). PGC1 α expression defines a subset of human melanoma tumors with increased mitochondrial capacity and resistance to oxidative stress. *Cancer Cell* 23, 287–301.
- Wakamatsu, K., Ito, S., and Rees, J.L. (2002). The usefulness of 4-amino-3-hydroxyphenylalanine as a specific marker of pheomelanin. *Pigment Cell Res.* 15, 225–232.
- Walton, R.T., Christie, K.A., Whittaker, M.N., and Kleinstiver, B.P. (2020). Unconstrained genome targeting with near-PAMless engineered CRISPR-Cas9 variants. *Science* 368, 290–296.
- Wang, Y. (2008). Bulky DNA lesions induced by reactive oxygen species. *Chem. Res. Toxicol.* 21, 276–281.
- Won, S., Morris, N., Lu, Q., and Elston, R.C. (2009). Choosing an optimal method to combine P-values. *Stat. Med.* 28, 1537–1553.
- Wu, X., and Hammer, J.A. (2014). Melanosome transfer: it is best to give and receive. *Curr. Opin. Cell Biol.* 29, 1–7.
- Yang, J., Lee, S.H., Goddard, M.E., and Visscher, P.M. (2011). GCTA: a tool for genome-wide complex trait analysis. *Am. J. Hum. Genet.* 88, 76–82.
- Zhang, Q., Padayatti, P.S., and Leung, J.H. (2017). Proton-Translocating Nicotinamide Nucleotide Transhydrogenase: A Structural Perspective. *Front. Physiol.* 8, 1089.
- Zhao, W.N., and McAlister-Henn, L. (1996). Assembly and function of a cytosolic form of NADH-specific isocitrate dehydrogenase in yeast. *J. Biol. Chem.* 271, 10347–10352.
- Zhao, T., Huang, X., Han, L., Wang, X., Cheng, H., Zhao, Y., Chen, Q., Chen, J., Cheng, H., Xiao, R., and Zheng, M. (2012). Central role of mitofusin 2 in autophagosome-lysosome fusion in cardiomyocytes. *J. Biol. Chem.* 287, 23615–23625.

STAR★METHODS

KEY RESOURCES TABLE

REAGENT or RESOURCE	SOURCE	IDENTIFIER
Antibodies		
anti-MITF monoclonal antibody C5	Made in the lab of Dr. David E. Fisher	King et al., 1999; C5
Mouse monoclonal anti-tyrosinase antibody, clone T311	Sigma-Aldrich	Cat# 05-647; RRID: AB_309873
Donkey anti-rabbit IgG-HRP	ThermoFisher Scientific	Cat# 45-000-683; RRID: AB_2721111
Amersham ECL mouse IgG, HRP	ThermoFisher Scientific	Cat#45000680; RRID: AB_2721110
Monoclonal anti-β-actin-peroxidase	Sigma Aldrich	Cat# A3854; RRID: AB_262011
Alexa Fluor 555 goat anti-rabbit IgG (H+L), secondary antibody	ThermoFisher Scientific	Cat# A-21428; RRID: AB_2535849
Alexa Fluor 647 goat anti mouse IgG (G+L); fluorescence conjugated secondary antibody	ThermoFisher Scientific	Cat# A-21236; RRID: AB_2535805
Alexa Fluor 594 F(ab)2 fragment of goat anti-rabbit IgG (G+L); fluorescence conjugated secondary antibody	ThermoFisher Scientific	Cat# A-11072; RRID: AB_2534116
Alexa Fluor 488-conjugated donkey anti-mouse secondary antibodies	ThermoFisher Scientific	Cat# A-21202; RRID: AB_141607
Anti-Cyclobutane Pyrimidine Dimers (CPDs) mAb antibody (Clone TDM-2)	Cosmo Bio USA	Cat# CAC-NM-DND-001; RRID: AB_1962813
Rabbit anti-γ-H2AX (P-ser139) polyclonal antibody	NOVUS Biologicals	Cat# NB100-384; RRID: AB_10002815
Mouse monoclonal anti-Mitofusin 2 antibody [6A8]	Abcam	Cat# ab56889; RRID: AB_2142629
Rabbit polyclonal anti TRP2/DCT antibody	Abcam	Cat# ab74073; RRID: AB_1524517
Mouse monoclonal anti-NNT antibody [8B4BB10]	Abcam	Cat# ab110352; RRID: AB_10887748
Rabbit anti-NNT (C-terminal) polyclonal antibody	Abcam	Cat# ab214212; RRID: AB_2889980
Mouse anti-8-oxo-dG monoclonal antibody	Trevigen	Cat# 4354-MC-050; RRID: AB_1857195
IDH1 (D2H1) Rabbit mAb	Cell Signaling Technology	Cat# 8137; RRID: AB_10950504
Mouse monoclonal p53 antibody [PAb 240]	Abcam	Cat# ab26; RRID: AB_303198
Rabbit monoclonal TRP1 antibody [EPR21960]	Abcam	Cat# ab235447; RRID: AB_2889980
Mouse monoclonal antibody Pmel17 (E-7)	Santa Cruz Biotechnology	Cat# sc-377325; RRID: AB_2889982
LC3B (D11) rabbit monoclonal antibody	Cell Signaling Technology	Cat#38668S RRID: AB_2137707
Biological samples		
Full thickness human breast and abdominal skin explants	Massachusetts General Hospital	IRB# 2013P000093
Paraffin-embedded formalin fixed slides, prepared from breast and abdominal biopsy samples	Massachusetts General Hospital	IRB# 2013P000093
Human skin samples for genome wide association study (GWAS)	Massachusetts General Hospital or the Cooperative Human Tissue Network	IRB# 2013P000093
Chemicals, peptides, and recombinant proteins		
3-isobutyl-1-methylxanthine (IBMX)	Sigma-Aldrich	Cat# I5879
12-O-tetradecanoylphorbol-13-acetate (TPA)	Sigma-Aldrich	Cat# 16561-29-8
Ham's F10	Thermo Fisher Scientific	Cat# MT10070CV
N6,2'-O-Dibutyryladenine 3',5'-cyclic monophosphate sodium salt	Sigma-Aldrich	Cat# D0627
Penicillin-Streptomycin	Thermo Fisher Scientific	Cat# 15140163
Na3VO4	Sigma-Aldrich	Cat# 450243
Medium 254	Life Technologies	Cat# M254500
0.05% Trypsin-EDTA w/ phenol red	Life Technologies	Cat# 25300120
Human Melanocyte Growth Supplement (HMGS)	Life Technologies	Cat# S0025

(Continued on next page)

Continued

REAGENT or RESOURCE	SOURCE	IDENTIFIER
Bovine Serum Albumin	Sigma	Cat#A7030
Goat serum	Sigma-Aldrich	Cat# G9023
RPMI (Roswell Park Memorial Institute 1640 Medium)	Life Technologies	Cat# 11875119
RIPA lysis buffer	Sigma-Aldrich	Cat# R0278
FetalPlex Animal Serum Complex	Gemini Bio-Products	Cat# 100-602
Western Lightning Plus-ECL	PerkinElmer	Cat # NEL105001EA
Non-fat milk powder	Boston BioProducts	Cat# P-1400
Protein Block	Agilent	Cat# X090930-2
Antibody Diluent	DAKO	Cat# S3022
VECTASHIELD® HardSet Antifade Mounting Medium with DAPI	Vector Laboratories	Cat# H-1500
synthetic melanin	Sigma Aldrich	Cat# M8631
N,N-Dicyclohexylcarbodiimide [DCC]	Sigma Aldrich	Cat# D80002
2,3-Butanedione [2,3BD]	Sigma Aldrich	Cat# B85307
Palmitoyl coenzyme A lithium salt	Sigma Aldrich	Cat# #P9716
cycloheximide (CHX)	Sigma Aldrich	Cat# C7698
NADPH	Sigma Aldrich	Cat# N7505
N-Acetyl-L-cysteine (NAC)	Sigma Aldrich	Cat# A7250
MitoTEMPO	ThermoFisher Scientific	Cat# 501872447
Hydrogen peroxide solution	Sigma Aldrich	Cat# 216763
SYBR FAST qPCR master mix	Kapa Biosystems	Cat# KK4600;
Protease and Phosphatase Inhibitor	ThermoFisher Scientific	Cat# P178445
Western Lightning Plus-ECL, Enhanced Chemiluminescence Substrate	Perkin Elmer	Cat# NEL105001EA
MitoSOX Red	ThermoFisher Scientific	Cat# M36008
CM-H2DCFDA	ThermoFisher Scientific	Cat# C6827
NucBlue	ThermoFisher Scientific	Cat# R37605
Polybrene	Sigma-Aldrich	Cat# TR-1003
Paraformaldehyde 16%	ThermoFisher Scientific	Cat# 50980487
Ethanol	Thermo Fisher Scientific	Cat# 04355226
Triton X-100	Sigma Aldrich	Cat# T8787
TWEEN® 20	Sigma Aldrich	Cat# P7949
Forskolin from Coleus forskohlii, ≥ 98%	Sigma Aldrich	Cat# F6886
Lipofectamine RNAiMAX Transfection Reagent	Life Technologies	Cat# 13778150
IQ5 High-fidelity DNA Polymerase	New England Biolabs	Cat# M0491S
Critical commercial assays		
Direct cAMP ELISA Kit	Enzo Life Sciences	Cat# ADI-901-066
GSH/GSSG-Glo Assay	Promega	Cat# V6611
CellTiter-Glo Luminescent Cell Viability Assay	Promega	Cat# G7570
Pierce BCA protein assay	ThermoFisher Scientific	Cat# 23225
KAPA Library Quantification Kits	Roche	Cat# 7960140001
MiSeq Reagent Kits v2 (300 cycles)	Illumina	Cat# MS-102-2002
MaxBlock Autofluorescence Reducing Reagent Kit	MaxVision Biosciences	Cat# MB-L
Fontana-Masson Stain Kit (Melanin Stain)	Abcam	Cat# ab150669
Dual Reporter System	GeneCopoeia	Cat# HPRM39435-LvPM02
Secrete-Pair Gaussia Luciferase Assay Kit	GeneCopoeia	Cat# LF062
NADP/NADPH-Glo Assay	Promega	Cat# G9082

(Continued on next page)

Continued

REAGENT or RESOURCE	SOURCE	IDENTIFIER
QUANTI-Blue Solution	InvivoGen	Cat# rep-qbs
RNeasy Plus Mini Kit	QIAGEN	Cat# 74136

Deposited data

Raw data supporting the human genetics association analyses		https://www.dropbox.com/scl/fi/ahdfnjo4puwzd8ayw2ix/supporting-data-human-genetic-associations-2.xlsx?dl=0&rkey=gvbpat4tjb6bnekgnxu1a6yh
---	--	---

Publicly available data

Ensembl database information for promoter ENSR00000180214 of the NNT gene	Ensembl	http://grch37.ensembl.org/Homo_sapiens/Regulation/Summary?fdb=funcgen;r=5:43600400-43606201;rf=ENSR00000180214
GTEX expression database	GTEX	https://www.gtexportal.org/
GWAS summary statistics from the CANDELA cohort	GWAS Central	https://www.gwascentral.org/study/HGVST3308
GWAS summary statistics from the UK Biobank cohort		https://cnsgenomics.com/software/gcta/#DataResource

Experimental models: cell lines

Primary human melanocytes (isolated from neonatal foreskins)	Massachusetts General Hospital	IRB# 2013P000093
Human melanoma cell line UACC257	National Cancer Institute Division of Cancer Treatment and Diagnosis (DCTD) Tumor Repository	
Human melanoma cell line SK-MEL-30	Memorial Sloan Kettering Cancer Center	https://www.mskcc.org/
Mouse Melan-A cell line	Wellcome Trust Functional Genomics Cell Bank	Bennett et al., 1987
Primary human keratinocytes isolated from discarded surgical human skin tissue (e.g., foreskins)	Massachusetts General Hospital	IRB# 2013P000093
Primary human fibroblasts isolated from discarded surgical human skin tissue (e.g., foreskins)	Massachusetts General Hospital	IRB# 2013P000093
Lenti-X 293T cells	Clontech	Cat# 632180

Experimental models: Organisms/strains

C57BL/6J mice	Jackson Laboratory	Stock No: 000664
C57BL/6NJ mice	Jackson Laboratory	Stock No: 005304
Casper zebrafish (<i>mitfa</i> ^{-/-} ; <i>roy</i> ^{-/-}) embryos	Laboratory of Dr. Leonard I. Zon	

Oligonucleotides

nheIkozakHAhNNT_f1: forward, 5'-ctagctagcCCGCCA CCATGTACCCATACGATGTTCCAGATTACGCTGCAA ACCTATTGAAAACAGTGGTGACTG-3'	euofins Genomics	For PLMJ1- HA-NNT
hNNTnheI_r1: reverse, 5'-ctagctagcTTACTTCTGATA GGATTCTCTAACCTTCGC-3'	euofins Genomics	For PLMJ1- HA-NNT
nheIkozakhMFN2_f1: forward, 5'-ctagctagcGCCACC ATGTCCCTGCTCTTCTCTCGATGC-3'	euofins Genomics	For PLMJ1- HA MFN2
hMFN2(HA)nheI_r1: reverse, 5'-ctagctagcTTAGGATC CAGCAGCGTAATCTGGAAC-3'	euofins Genomics	For PLMJ1- HA MFN2

RT-Primers for *NNT*, *IDH1*, *MFN2*, *TYRP1*, *DCT/TRP2*, *MITF*, *POMC*, *PPARGC1A*, *Tyrosinase*: See Table in STAR Methods

Additional oligonucleotides that were used for *nnt* knockout in zebrafish are in [Table S3](#)

(Continued on next page)

Continued

REAGENT or RESOURCE	SOURCE	IDENTIFIER
Recombinant DNA		
CRISPR MiniCoopR-U6:gRNA-mitfa:Cas9 plasmid	Addgene	Cloned from Addgene plasmid ID 118840
pMiniCoopR-mitfa:NNT expression plasmid	Addgene	Cloned from Addgene plasmid ID 118850
pLMJ1-NNT-HA	This manuscript	Based on Addgene plasmid, # 19319
pLMJ1-EGFP plasmid	Laboratory of Dr. David Sabatini	Addgene plasmid, # 19319; http://addgene.org/19319 ; RRID:Addgene_19319 (Sancak et al., 2008)
pcDNA3.1 Mfn2HA	Laboratory of Dr. Allan Weissman	Addgene plasmid, # 139192; http://addgene.org/139192 ; RRID:Addgene_139192 (Leboucher et al., 2012)
PLMJ1-MFN2-HA	This manuscript	Based on Addgene plasmid, # 139192 and Addgene plasmid, # 19319

Software and algorithms

GraphPad Prism 8.4.3 (471)	GraphPad	https://www.graphpad.com/scientific-software/prism/
ImageJ (v1.8.0)	National Institutes of Health	https://imagej.nih.gov/ij/
FIJI software for pixel-based color quantification	FIJI	https://imagej.net/Fiji
Off-target prediction software (for design of guide RNAs)	Bae et al., 2014	http://www.rgenome.net/cas-offinder/
On-target prediction software (for design of guide RNAs); CRISPRscan and CHOPCHOP	Moreno-Mateos et al., 2015; Labun et al., 2019	https://www.crisprscan.org/ ; https://chopchop.cbu.uib.no/
Axiovision REL 4.7 software	Zeiss	https://carl-zeiss-axiovision-rel.software.informer.com/4.7/
CRISPResso2 software (for genome editing)	Clement et al., 2019	
MACH software		http://csg.sph.umich.edu/abecasis/mach/index.html
GCTA program	Yang et al., 2011	https://cnsgenomics.com/software/gcta/
PLINK program		https://www.cog-genomics.org/plink/1.9/
BioRender		http://www.BioRender.com
Fiji	Saalfeld, S., Schmid, B., et al. (2012)	https://imagej.net/Fiji
NDP.view2 Viewing software	HAMAMATSU	https://www.hamamatsu.com/us/en/product/type/U12388-01/index.html

Other

siGENOME Human MITF siRNA SMARTpool	Dharmacon	Cat# M-008674-00-0005
ON-TARGETplus Human IDH1 siRNA SMARTpool	Horizon Inspired Cell Solutions	Cat# L-008294-01-0005
ON-TARGETplus Human MFN2 siRNA SMARTpool	Horizon Inspired Cell Solutions	Cat# L-012961-00-0005
ON-TARGETplus Human NNT siRNA SMARTpool	Horizon Inspired Cell Solutions	Cat# L-009809-00-0005
ON-TARGETplus Human PPRGC1A siRNA SMARTpool	Horizon Inspired Cell Solutions	Cat# L-005111-00-0005
ON-TARGETplus Human Tyrosinase siRNA SMARTpool	Horizon Inspired Cell Solutions	Cat# L-012555-00-0005
ON-TARGETplus non-targeting siRNA control pool	Horizon Inspired Cell Solutions	Cat# D-001810-10-05
4-15% Criterion TGX Precast Midi Protein gels	Bio-Rad Laboratories	Cat# 5671084
Chamber slides	ThermoFisher Scientific	Cat# 125657

RESOURCE AVAILABILITY

Lead contact

Further information and requests for resources and reagents should be directed to and will be fulfilled by the Lead Contact Elisabeth Roider (eroider@cbr2.mgh.harvard.edu).

Materials availability

Plasmids, mouse and zebrafish lines generated in this study will be distributed upon request to other investigators under a Material Transfer Agreement. All unique/stable reagents generated in this study are available from the Lead Contact with a completed Materials Transfer Agreement.

Data and code availability

All the Software packages and methods used in this study have been properly detailed and referenced under the Software and algorithms listed in [Key resources table](#). All Human data (SNP analysis) generated in this study are available under the Deposited data listed in [Key resources table](#).

EXPERIMENTAL MODEL AND SUBJECT DETAILS

Ethics Statement

Mice studies and procedures were approved by the Institutional Animal Care and Use Committee of Massachusetts General Hospital and were conducted strictly in accordance with the approved animal handling protocol. Zebrafish experiments performed in this study were in strict accordance with the recommendations in the Guide for the Care and Use of Laboratory Animals of the National Institutes of Health. The animal research protocol, including zebrafish maintenance and euthanasia was approved by the Institutional Animal Care and Use Committee of Boston Children's Hospital.

Mice

All mice were bred on a heterozygous MiWhite background (*Mitf* white) (Steingrímsson et al., 2004). C57BL/6J mice (Jackson Laboratory, Stock No: 000664) displaying a 5-exon deletion in the *Nnt* gene resulting in a homozygous loss were compared to *Nnt* wild-type C57BL/6NJ mice (Jackson Laboratory, Stock No: 005304). All mice were matched by gender and age (female, 6 weeks old). Mice were genotyped according to the protocol obtained from Jackson Laboratory (protocol 26539: Standard PCR Assay - *Nnt* < C57BL/6J > , Version 2.2).

Zebrafish

Overexpression of human NNT in Zebrafish

The human *NNT* gene was cloned into the MiniCoopR expression plasmid to allow melanocyte-specific overexpression of *NNT* (Ceol et al., 2011). The MiniCoopR plasmid contains an *mitf* mini-gene alongside *mitfa* driven *NNT* or an empty control. Casper zebrafish (*mitfa*−/−; *roy*−/−) embryos (Ablain et al., 2015) were injected at the single cell stage with plasmid DNA, which gets incorporated into the genome through Tol2 transgenesis. This results in the rescue of melanocytes via the *mitfa* minigene and melanocyte-specific overexpression of *NNT*. Larvae were raised for 5 days and imaged using a Nikon SMZ18 Stereomicroscope.

Deletion of Zebrafish *nnt* gene

SpCas9 guide RNAs (gRNAs) were designed to target the first two exons of the zebrafish *nnt* gene using on-target and off-target prediction software (Table S3). gRNA expression plasmids were constructed by cloning oligonucleotides (Integrated DNA Technologies) into BseRI-digested pMiniCoopR-U6:gRNA-*mitfa*:Cas9 (Addgene plasmid ID 118840) (Ablain et al., 2015). A control CRISPR MiniCoopR plasmid was generated by cloning a scrambled gRNA into the CRISPR MiniCoopR vector. The CRISPR MiniCoopR plasmid contains an *mitf* mini-gene alongside *mitfa*:Cas9 and U6:gRNA. Casper zebrafish (*mitfa*−/−; *roy*−/−) embryos (Ablain et al., 2015) were injected at the single cell stage with plasmid DNA, which gets incorporated into the genome through Tol2 transgenesis. This results in the rescue of melanocytes via the *mitfa* minigene and melanocyte-specific knockout of *nnt*. Larvae were raised for 4 days and imaged using a Nikon SMZ18 Stereomicroscope.

DNA was extracted from the embryos at 4 days post fertilization using the Hot Shot method (Truett et al., 2000), for analysis of genome editing. The efficiency of genome modification by SpCas9 was determined by next-generation sequencing using a 2-step PCR-based Illumina library construction method, as previously described (Walton et al., 2020). Briefly, genomic loci were amplified from gDNA extracted from pooled samples of 8-10 zebrafish embryos using Q5 High-fidelity DNA Polymerase (New England Biolabs, # M0491S) with the primers listed in Table S3. PCR products were purified using paramagnetic beads prepared as previously described (Rohland and Reich, 2012; Kleinstiver et al., 2019). Approximately 20 ng of purified PCR product was used as template for a second PCR to add Illumina barcodes and adaptor sequences using Q5 and the primers (Table S3). PCR products were purified prior to quantification via capillary electrophoresis (QIAGEN QIAxcel), followed by normalization and pooling. Final libraries were quantified by qPCR using a KAPA Library Quantification Kit (Roche, #7960140001) and sequenced on a MiSeq sequencer using a 300-cycle v2 kit (Illumina, #MS-102-2002). Genome editing activities were determined from the sequencing data using CRISPResso2 (Clement et al., 2019) with default parameters.

Chemical treatment of Zebrafish

Wild-type Tübingen zebrafish (Figure 4D) or *mcr*:NNT or *mcr*:Empty rescued Casper Zebrafish (Figure S5C) were placed in a 24 well plate at 72 hours post-fertilization, with 10 larvae per well for a total twenty larvae per condition. Larvae were treated for 24 hours with either 2,3BD (1 μ M, 10 μ M, 100 μ M, 1 mM; Sigma Aldrich, #B85307), DCC (1 μ M, 10 μ M, 50 μ M, 100 μ M; Sigma Aldrich, #D80002), or

DMSO (1:500) in E3 embryo medium. At 4 days post fertilization, larvae were imaged using a Nikon SMZ18 Stereomicroscope. At least 57 melanocytes from 18 zebrafish embryos were analyzed using the FIJI software enabling pixel-based color quantification.

Quantification of pigmentation in the Zebrafish model

Pigmentation of free-standing melanocytes were identified at high magnification, making sure no overlapping signal was included into the analysis. The intra-melanocytic region was marked and the brightness was measured using the FIJI software. The measured output is the mean pixel intensity of the measured region (= melanocyte), which was plotted as one dot in the graph displayed.

Human skin explants

Skin samples considered surgical waste were obtained de-identified from healthy donors (IRB# 2013P000093) undergoing reconstructive surgery, according to institutional regulations. Full thickness human abdominal skin explants were cultured in Petri dishes with a solid phase and liquid phase phenol red free DMEM medium containing 20% penicillin/streptomycin/glutamine, 5% fungizone (GIBCO), and 10% fetal bovine serum. Explants were treated with vehicle (DMSO), 2,3BD (50 mM, 1 M, or 11 M); or DCC (50 mM) as indicated in the figure legends. Compounds were applied strictly on top of the explants, making sure no drip occurred into the underlying media. For UV irradiation experiments, a UV lamp (UV Products) was used at 1000 mJ/cm² UVB.

Cell lines

Primary human melanocytes were isolated from normal discarded foreskins and were established in TIVA medium as described previously (Khaled et al., 2010) or in Medium 254 (Life Technologies, #M254500) (Allouche et al., 2015). Human melanoma cell line UACC257 (sex unspecified) was obtained from the National Cancer Institute (NCI), Frederick Cancer Division of Cancer Treatment and Diagnosis (DCTD) Tumor Cell Line Repository. SK-MEL-30 (male) human melanoma cell line was from Memorial Sloan Kettering Cancer Center. Both melanoma cell lines have been authenticated by our lab using ATCC's STR profiling service. UACC257 and SK-MEL-30 cells were cultured in DMEM and RPMI medium (Life Technologies, #11875119) respectively, supplemented with 10% fetal bovine serum and 1% penicillin/streptomycin/L-glutamine in a humidified atmosphere of 95% air and 5% CO₂ at 37°C.

Murine Melan-A (Bennett et al., 1987) cells were obtained from the Wellcome Trust Functional Genomics Cell Bank. Melan-A cells were grown in RPMI 1640 supplemented with 10% FBS or FetalPlex (Gemini Bio-Products, #100-602), 100,000 U/L penicillin, 100 mg/L streptomycin sulfate, 100x Glutamax, and 200 nM TPA.

Primary human keratinocytes were cultured in EpiLife® medium supplemented with human keratinocyte growth supplement (HKGS, ThermoFisher Scientific). Primary human fibroblasts were cultured in medium 106 supplemented with low serum growth supplement (LSGS, ThermoFisher Scientific). 10⁶ and 10⁴ cells were plated per well of 6-well and 96-well plates, respectively. Drugs indicated in the figure legends were dissolved in DMSO and added 1:1000 to the culture media for 24 h at the concentrations indicated.

METHOD DETAILS

siRNA transfection

A single treatment of 10 nmol/L of siRNA was delivered to a 60% confluent culture by transfection with Lipofectamine RNAiMAX (Life Technologies, #13778150) according to the manufacturer's recommendations. After 48-72 h of transfection, total RNA or protein was harvested.

Plasmid overexpression

Human *NNT* fused to a haemagglutinin (HA)-tag at the N terminus was amplified from pEGFP-C1-h*NNT* (primer sequences are in the [Key resources table](#)) and was subcloned into the *NheI* restriction site of pLJM1-EGFP [a gift from David Sabatini, Addgene plasmid #19319; <http://addgene.org/19319>; RRID:Addgene_19319; Sancak et al., 2008] using *NheI* (New England Biolabs, R3131S).

For human MFN2 overexpression, human *MFN2* fused to three HA tags at the C terminus was amplified from pcDNA3.1 Mfn2HA (a gift from Allan Weissman, Addgene plasmid 139192; <http://addgene.org/139192>; RRID:Addgene_139192; Lebouche et al., 2012) (primer sequences are in the [Key resources table](#)) and was subcloned into the *NheI* restriction site of pLJM1-EGFP using *NheI* (New England Biolabs, #R3131S).

FLAG-tagged human *NNT* cDNA (*NNT*-FLAG) was purchased from Origene (RC224002). The *NNT*-FLAG cassette was re-cloned into pLJM1-EGFP (Addgene #19319) following *NheI* and *EcoRI* digestion.

Lentivirus generation and infection

Lentivirus was generated in Lenti-X 293T cells (Clontech, #632180). The Lenti-X cells were transfected using 250 ng pMD2.G, 1250 ng psPAX2, and 1250 ng lentiviral expression vector in the presence of PEI (MW:25K). For infection with lentivirus, 0.1–1 mL of lentivirus-containing medium was used in the presence of 8 µg/ml polybrene (Sigma, #TR-1003). Selection with puromycin (10 µg/ml) was performed the day after infection.

In vitro culture with NNT inhibitors

2,3-Butanedione 97% (2,3 BD) (Sigma Aldrich, #B85307) (1 μ M, 10 μ M, 100 μ M, 2 mM), N,N-Dicyclohexylcarbodiimide (DCC) (Sigma Aldrich, #D80002) (1 mM, 2 mM, 10 mM), and Palmitoyl coenzyme A lithium salt (Sigma Aldrich, #P9716) (10 μ M, 2 mM) were reconstituted with DMSO (American Type Culture Collection, 4-X).

Immunoblotting

Whole-cell protein lysates were prepared using RIPA lysis buffer (Sigma-Aldrich, #R0278) supplemented with Protease and Phosphatase Inhibitor (ThermoFisher Scientific, #PI78445). Protein concentrations were quantified using the Pierce BCA protein assay (ThermoFisher Scientific, #23225). Immunoblotting was performed by standard techniques using 4%–15% Criterion TGX Precast Midi Protein gels (Bio-Rad Laboratories, #5671084) and transferring to 0.2 μ m nitrocellulose membranes (Bio-Rad Laboratories, #1620112). Membranes were blocked with 5% non-fat milk (Boston BioProducts, #P-1400) in PBS containing 0.1% Tween 100 and incubated with one of the following primary antibodies at the indicated dilution (antibody sources are in the [Key resources table](#)): 1:20 dilution of anti-MITF monoclonal antibody C5, 1:1,000 dilution of anti-Tyrosinase clone T311, 1:1,000 dilution of anti-Mitofusin-2 antibody [6A8], 1:500 dilution of TRP2/DCT antibody, 1:1,000 dilution of anti-NNT antibody [8B4BB10], 1:1,000 dilution of anti-IDH1 (D2H1) antibody, 1:1,000 dilution of p53 antibody [PAb 240], 1:1,000 dilution of TYRP1 antibody [EPR21960], 1:1,000 dilution of mouse monoclonal antibody Pmel17 (E-7), or 1:1,000 dilution of LC3B (D11) rabbit monoclonal antibody. Incubation with the appropriate secondary antibody followed, either a 1:5,000 dilution of donkey anti-Rabbit IgG-HRP or a 1:3,000 dilution of Amersham ECL mouse IgG, HRP.

To verify equal loading of samples, membranes were re-probed with a 1:20,000 dilution of monoclonal anti- β -actin-peroxidase (Sigma Aldrich, #A3854). Protein bands were visualized using Western Lightning Plus ECL (PerkinElmer, #NEL105001EA) and quantified using ImageJ software (NIH).

RNA purification and quantitative RT-PCR

Total RNA was isolated from cultured primary melanocytes or melanoma cells at the indicated time points, using the RNeasy Plus Mini Kit (QIAGEN, #74136). mRNA expression was determined using intron-spanning primers with SYBR FAST qPCR master mix (Kapa Biosystems, #KK4600).

Expression values were calculated using the comparative threshold cycle method ($2^{-\Delta\Delta C_t}$) and normalized to human *RPL11* mRNA. The primers used for quantitative RT-PCR (euofins Genomics) and are listed below.

Primer	Sequence
Human <i>RPL11</i> : forward	5'-GTTGGGGAGAGTGGAGACAG-3'
Human <i>RPL11</i> : reverse	5'-TGCCAAAGGATCTGACAGTG-3'
Human <i>M isoform MITF</i> : forward	5'-CATTGTTATGCTGGAAATGCTAGAA-3'
Human <i>M isoform MITF</i> : reverse	5'-GGCTTGCTGTATGTGGTACTTGG-3'
Human Tyrosinase: forward	5'-ACCGGGAATCCTACATGGTTCCTT-3'
Human Tyrosinase: reverse	5'-ATGACCAGATCCGACTCGTTGTT-3'
Human NNT: forward	5'-AGCTCAATACCCATTGCTG-3'
Human NNT: reverse	5'-CACATTAAGCTGACCAGGCA-3'
Human IDH1: forward	5'-GTC GTCATGCTTATGGGG AT-3'
Human IDH1 reverse	5'-CTT TTGGGTTCCGTCCT TG-3'
Human MFN2: forward	5'-CTG CTA AGG AGGTGCTCA A-3'
Human MFN2: reverse	5'-TCC TCA CTTGAAAGC CTT CTG C-3'
Human PPARGC1A: forward	5'-CTG CTA GCA AGTTTG CCT CA-3'
Human PPARGC1A: reverse	5'-AGTGGTGCAAGTACCAATCA-3'
Human POMC: forward	5'-AAGAGGCTAGAGGTCATCAG-3'
Human POMC: reverse	5'-AGAACGCCATCATCAAGAAC-3'
Human TYRP1 forward	5'-CCAGTCACCAACACAGAAATG-3'
Human TYRP1 reverse	5'-GTGCAACCAGTAACAAAGCG-3'
Human TRP2/DCT forward	5'-TTCTCACATCAAGGACCTGC-3'
Human TRP2/DCT reverse	5'-ACACATCACACTCGTTCCTC-3'

Cycloheximide chase assay

72 h after siRNA transfection (siControl or siNNT), UACC257 melanoma cells were treated with a protein synthesis inhibitor, cyclohexamide (CHX, Sigma Aldrich #C7698, 50 $\mu\text{g}/\text{ml}$), for the indicated times and then immediately subjected to immunoblotting for tyrosinase protein expression. The expression of tyrosinase was quantified using ImageJ software based on band intensities and normalized to the intensities of the corresponding β -actin bands. The normalized tyrosinase expression was then defined as relative tyrosinase expression by setting the mean values at $t = 0$ in each experimental group to 1.0.

In the ROS rescue experiments, siRNA-containing medium was replaced with fresh culture medium containing either N-acetyl-L-cysteine (NAC; Sigma Aldrich #A7250, 5 mM), β -nicotinamide adenine dinucleotide 2'-phosphate (NADPH; Sigma Aldrich #N7505, 0.1 mM), MitoTEMPO (ThermoFisher #501872447, 20 μM) or control vehicle (DMSO or TrisHCl respectively) 24h after siRNA transfection. The siRNA-transfected cells were cultured for an additional 48 h in the presence of these agents and then examined by the CHX chase assay as described above.

pLJM-1-EGFP or pLJM1-NNT/FLAG was introduced into UACC257 cells using Lipofectamine 3000. 48 h after transfection, the transfection medium was replaced with fresh medium containing DMSO or 10 μM MG132 (Sigma Aldrich #M8699) and pre-incubated for 6 h. Then, CHX was added to assess tyrosinase protein stability as described above.

Melanin quantification

Equal numbers of cells were plated in 6-well plates. The cells were then harvested 72 – 96 hours post siRNA or NNT inhibitors compounds, as indicated in the legends, pelleted, washed in PBS and counted. 10^6 cells were used for measurement of protein concentration with the Pierce BCA protein assay (Thermo Fisher Scientific, #23225) and 10^6 cells were resuspended in 60 μL of 1 N NaOH solution and incubated at 60°C for 2 h or until the melanin was completely dissolved. After cooling down to room temperature, samples were centrifuged at $500 \times g$ for 10 min and the supernatants were loaded onto a 96-well plate. The melanin content was determined by measuring the absorbance at 405 nm on an Envision plate reader, compared with a melanin standard (0 to 50 $\mu\text{g}/\text{ml}$; Sigma Aldrich, #M8631). Melanin content was expressed as micrograms per milligram of protein.

Eumelanin and pheomelanin analysis

Lyophilized cells (1×10^6) from human abdominal full thickness skin explants were ultrasonicated in 400 μL of water and fur samples were homogenized at a concentration of 10 mg/mL in water in a Ten-Broeck homogenizer. Aliquots of 100 μL were subjected to alkaline hydrogen peroxide oxidation to yield the eumelanin marker, pyrrole-2,3,5-tricarboxylic acid (PTCA) (Ito et al., 2011), or to hydroiodic acid (HI) hydrolysis to yield the pheomelanin marker, 4-amino-3-hydroxyphenylalanine (4-AHP) (Wakamatsu et al., 2002), then the samples were analyzed by HPLC. Amounts of each marker are reported as ng of marker per 10^6 cells or mg fur. Pheomelanin and eumelanin contents were calculated by multiplying the 4-AHP and PTCA contents by factors of 7 and 25, respectively (d'Ischia et al., 2013).

Skin colorimeter measurements

Skin reflectance measurements were made using a CR-400 Colorimeter (Minolta Corporation, Japan). Before each measurement, the instrument was calibrated against the white standard background provided by the manufacturer. The degree of melanization (darkness) is defined as the colorimetric measurement on the *L axis (luminance, ranging from completely white to completely black) of the Centre Internationale d'Éclairage (CIE) $L^*a^*b^*$ color system (Park et al., 1999). Each data point is the mean of measurements performed in technical triplicate (three different locations within the same ear).

Determination of intracellular cAMP content

Cyclic adenosine monophosphate (cAMP) was measured directly using an enzyme-linked immunosorbent assay (ELISA) (Enzo Life Sciences, #ADI-901-066). cAMP was quantified in 100,000 cells based on a standard curve.

Cell viability assay

Human melanoma cell lines and isolated primary cultured human melanocytes were propagated and tested in early passage (Passages 7 to 9). The effects of NNT inhibitors (2,3BD, DCC, and Palmitoyl coenzyme A lithium salt) on cell viability were evaluated by the CellTiter-Glo Luminescent Cell Viability Assay (Promega, #G7570) and measurement of luminescence was performed on an EnVision 2104 Multilabel Reader (PerkinElmer). Human melanoma cell lines and primary melanocytes were plated on 96-well white plates (10,000 cells/well) and were treated with the NNT inhibitors at the indicated concentrations for 24 h.

Glutathione measurements

Cell lysates were prepared from equal numbers of cells after 24 h of DCC or 2,3BD treatment, following the manufacturer's protocols. Seventy-two h post siRNA treatment or overexpression of NNT and their corresponding controls, glutathione levels were determined using the GSH/GSSG-Glo assay (Promega, #V6611) and luminescence was measured using an EnVision 2104 Multilabel Reader (PerkinElmer).

Determination of NADPH/NADP ratio

Cell lysates were prepared from equal numbers of UACC257 human melanoma cells 72 h post siRNA treatment or overexpression of NNT and their corresponding controls. NADPH/NADP⁺ ratios were determined using the NADP/NADPH-Glo Assay (Promega, #G9082) following the manufacturer's protocol and luminescence was measured using an EnVision 2104 Multilabel Reader (PerkinElmer).

Luciferase reporter assay

To measure MITF transcriptional activity, UACC257 melanoma cell lines were infected with the dual-reporter system (GeneCopoeia, #HPRM39435-LvPM02), which expresses secreted Gaussia luciferase (GLuc) under the TRPM1 promoter and SEAP (secreted alkaline phosphatase) as an internal control for signal normalization. The cells were grown in complete RPMI medium containing 10% Fetal Plex. Medium was collected 24, 48, and 72 h post siRNA transfection. GLuc and SEAP activities were measured by Secrete-Pair Gaussia Luciferase Assay Kit (GeneCopoeia, #LF062) and QUANTI-Blue Solution (Invivogen, #rep-qbs), respectively, according to the manufacturers' instructions.

Histology and Immunofluorescence

For histology, paraffin sections were prepared and stained with hematoxylin and eosin (H&E) using the ihisto service (<https://www.ihisto.io/>). For visualization of melanin, paraffin sections were stained using a Fontana-Masson Stain kit (abcam, #ab150669). Briefly, the samples were incubated in warmed Ammoniacal silver solution for 30 min, followed by a Nuclear Fast Red stain.

For immunofluorescence, paraffin sections were deparaffinized by xylene and rehydrated gradually with ethanol to distilled water. Sections were submerged in 0.01 M citrate buffer and boiled for 10 min for retrieval of antigen. The sections were washed with TBST (0.1% Tween 20) and blocked with protein blocking solution (Agilent, #X090930-2) for 1 h at room temperature before application of primary antibody [1:100 diluted in Antibody Diluent (DAKO, #S3022)] and incubation overnight at 4°C. The following day, sections were washed with TBST three times and incubated with secondary antibody Alexa Fluor 647 goat anti-mouse IgG (G+L) (ThermoFisher Scientific, #A-21236), Alexa Fluor 594 F(ab)₂ fragment of goat anti-rabbit IgG (G+L) (ThermoFisher Scientific, #A-11072), or Alexa Fluor 555 goat anti-rabbit IgG (ThermoFisher Scientific, #A-21428). After washing, the tissue sections were coverslipped with mounting medium (SlowFade® Gold Antifade Reagent with DAPI, ThermoFisher Scientific, #S36939). MaxBlock Autofluorescence Reducing Reagent Kit (MaxVision Biosciences, #MB-L) was used to quench skin tissue autofluorescence according to the reagent instructions.

The following primary antibodies were used at the indicated dilutions (antibody sources are in the Key Resources Table): anti-CPDs monoclonal antibody (1:1,500), rabbit anti- γ -H2AX (P-ser139) polyclonal antibody (1:5,000), rabbit anti-NNT (C-terminal) polyclonal antibody (1:100), rabbit anti- γ -H2AX [p Ser139] polyclonal antibody (1:100).

Primary human melanocytes (50,000 cells/well) were cultured on chamber slides (ThermoFisher Scientific, #125657). Seventy-two hours post siRNA transfection, the cells were fixed with 4% paraformaldehyde (PFA) (ThermoFisher Scientific, #50980487) for 20 min at room temperature, followed by treatment with 0.1% Triton X-100 (Sigma) for 5 min and blocking with 10% goat serum (Sigma Aldrich, #G9023) containing 5% BSA in PBS for 60 min at room temperature. Mouse anti-NNT monoclonal antibody [8B4BB10] was diluted with the blocking solution to a final concentration of 5 μ g/ml and incubated with the cells overnight at 4°C. The following day, the slides were washed with TBST three times and incubated with donkey anti-mouse Alexa Fluor 488 secondary antibody (1:500). Sections were washed with TBST three times and mounted in mounting medium (VECTASHIELD® HardSet Antifade Mounting Medium with DAPI, Vector Laboratories, #H-1500). Images were captured using confocal microscopy (Zeiss Axio Observer Z1 Inverted Phase Contrast Fluorescence microscope).

Detection of cellular reactive oxygen species (ROS)

The redox-sensitive fluorescent dye chloromethyl-2', 7'-dichlorodihydrofluorescein diacetates (CM-H2DCFDA, ThermoFisher Scientific, #C6827) was used to measure intracellular ROS accumulation. UACC257 melanoma cells were cultured on a glass bottom dish and treated with the indicated siRNAs. Forty-eight h post siRNA treatment, 2 μ M CM-H2DCFDA in PBS/5% FBS was added and the samples were incubated at 37°C for 30 min to assess overall ROS production. Subsequently, the cells were incubated with 5 μ M MitoSOX Red (ThermoFisher Scientific, #M36008) in PBS/5% FBS at 37°C for 10 min, washed with HBSS, and analyzed by immunofluorescence imaging (Zeiss Axio Observer Z1 Inverted Phase Contrast Fluorescence microscope). The results were normalized to cell numbers, which were determined by nuclear staining with 1 drop per ml of NucBlue (ThermoFisher Scientific, #R37605) at 37°C for 15 min.

Transmission electron microscopy

Cultured primary human melanocytes were grown in Medium 254 in 6-well transwell plates. Ninety-six h post siRNA or overexpression treatment, the cells were fixed with a modified Karnovsky's fixative (2% paraformaldehyde/2.5% glutaraldehyde in 0.1 M sodium cacodylate buffer, pH 7.4) for at least 2 h on a gentle rotator, followed by rinsing several times with 0.1 M cacodylate buffer. Then, the cells were treated with 1% osmium tetroxide/0.1 M cacodylate buffer for 1 h, rinsed thoroughly in 0.1 M cacodylate buffer, scraped, and the cell suspensions were transferred into 15 mL centrifuge tubes and centrifuged (3,000 rpm) for 15 min at 4°C. Pelleted material was embedded in 2% agarose, dehydrated through an ethanol gradient (series of solutions from 30% to 100% ethanol), dehydrated briefly

in 100% propylene oxide, then allowed to infiltrate overnight on a gentle rotator in a 1:1 mix of propylene oxide and Eponate resin (Ted Pella, Inc., kit with DMP30, #18010^o). The following day, specimens were transferred into fresh 100% Eponate resin for 2-3 hours, then embedded in flat molds in 100% fresh Eponate resin, and embeddings were allowed to polymerize for 24-48 h at 60°C. Thin (70 nm) sections were cut using a Leica EM UC7 ultramicrotome, collected onto formvar-coated grids, stained with 2% uranyl acetate and Reynold's lead citrate, and examined in a JEOL JEM 1011 transmission electron microscope at 80 kV. Images were collected using an AMT digital imaging system with proprietary image capture software (Advanced Microscopy Techniques, Danvers, MA).

Melanosomes-mitochondria distance measurements

Measurements of distances between melanosomes and mitochondria were quantified in FIJI (ImageJ) (Schindelin et al., 2012) by applying a customized macro to TEM micrographs. Melanosomes (N = ~50) were randomly selected for each condition within the whole image dataset. Thirty Euclidean distances from the melanosome surface to the closest mitochondria surface were measured in nm. From these 30 single measurements the mean was calculated to give a final single mean value per melanosome-mitochondria event. A total of ~50 events (N) were quantified per condition. Data were plotted and statistically analyzed using Prism 8 (Version 8.4.3). Melanosome-mitochondria distances closer than 20 nm were considered melanosome-mitochondria close appositions or contacts, consistent with (Daniele et al., 2014). Cell area (μm^2), number of melanosome-mitochondria contacts, and number of mitochondria were quantified in FIJI (ImageJ) using polygon and multi-point selection tools.

Melanosome stage quantification

Melanosome identification and quantification were performed with images at 40,000 x magnification or higher. Stages were estimated based on morphological features previously noted, namely multivesicular endosomes (Stage I), unpigmented fibrils (Stage II), pigmented fibrils (stage III), and darkly pigmented filled melanosomes (Stage IV). All identifiable melanosomes in 4 cells per condition were quantified and classified, and the proportions of each stage were normalized to cell cytosolic area (determined by ImageJ).

Tyrosinase activity assay

UACC257 human melanoma cells were treated with human NNT siRNA or non-targeting siRNA control pool for 4 days. Cell lysates were prepared by adding 1% Trion X100 in PBS for 1 h at room temperature with shaking. Tyrosinase activity was measured as previously described (Iozumi et al., 1993). Briefly, freshly made 25 mM L-DOPA in PBS was heated and added to the cell lysates in a 96-well plate. L-DOPA levels were determined by measuring the absorbance at 490 nm with shaking for 30 cycles, compared with mushroom tyrosinase (Sigma-Aldrich #T3824, 0 to 50 $\mu\text{g}/\mu\text{l}$ in PBS), using an Envision 2104 Multilabel plate reader (PerkinElmer).

Human genetic association studies

For all cohorts, the GRCh37/hg19 human genome build was used. SNPs with minor allele frequency less than 1% were excluded from each cohort.

Ethics Approval

Rotterdam study

The Medical Ethics Committee of the Erasmus Medical Center and the review board of the Dutch Ministry of Health, Welfare and Sports have ratified the Rotterdam study. Written informed consent was obtained from all participants.

East and South Africa

As detailed in Crawford et al. (2017), individuals used in the study were sampled from Ethiopia, Tanzania and Botswana. IRB approval for this project was obtained from the University of Pennsylvania. Written informed consent was obtained from all participants and research/ethics approval and permits were obtained from the following institutions prior to sample collection: the University of Addis Ababa and the Federal Democratic Republic of Ethiopia Ministry of Science and Technology National Health Research Ethics Review Committee; COSTECH, NIMR and Muhimbili University of Health and Allied Sciences in Dar es Salaam, Tanzania; the University of Botswana and the Ministry of Health in Gaborone, Botswana.

A. The Rotterdam Study

Population

The Rotterdam Study (RS) is a prospective population-based follow-up study of the determinants and prognosis of chronic diseases in middle age and elderly participants (aged 45 years and older) living in the Ommoord district (Rotterdam, the Netherlands) (Ikram et al., 2017). The RS consists of 4,694 people of predominantly North European ancestry.

Phenotyping

As part of the dermatological investigation within the RS, participants from three cohorts (RSI, RSII and RSIII) were screened to assess their skin color. In brief, trained physicians scored the skin color of the participants using a scale from 1 to 6, with 1 for albino, 2 for white, 3 for white to olive color, 4 for light brown, 5 for brown, and 6 for dark brown to black. The reliability of the assessment has been validated before (Jacobs et al., 2015). Individuals with dark skin were excluded since they were likely to have a different genetic background than Europeans.

Genotyping and imputation

The RS-I and RS-II cohorts were genotyped with the Infinium II HumanHap550K Genotyping BeadChip version 3 (Illumina, San Diego, California USA) and the RS-III cohort was genotyped using the Illumina Human 610 Quad BeadChip. The RS-I, RS-II and RS-III cohorts were imputed separately using 1000 Genomes phase 3 (Abecasis et al., 2012) as the reference dataset. Quality control on the single nucleotide polymorphisms (SNPs) has been described before (Hofman et al., 2015). SNPs were filtered out if they had a minor allele frequency of less than 1% or an imputation quality (R²) of less than 0.3. We used MACH software for the imputation with parameter defaults. Best-guess genotypes were called using the GCTA program (Yang et al., 2011) with parameter defaults.

Statistical analysis

We used a multivariate linear regression model to test for associations between SNPs within the *NNT* region and skin color in the RS using an additive model (Purcell et al., 2007). The model was adjusted for age, sex and four principal components (variables derived from principal component analysis that were added to correct for possible population stratification and hidden relatedness between participants). The PLINK program was used for conducting associations.

B. The CANDELA cohort

A GWAS study of skin color in the CANDELA cohort has been published (Adhikari et al., 2019) and summary statistics are available at <https://www.gwascentral.org/study/HGVST3308>. Details of the cohort and analyses are in the published study, so only the cohort population and phenotyping are summarized here.

Population

6,357 Latin American individuals were recruited in Brazil, Chile, Colombia, Mexico and Peru. Participants were mostly young, with an average age of 24.

Phenotyping

A quantitative measure of constitutive skin pigmentation (the Melanin Index, MI) was obtained using a DermaSpectrometer DSMEII reflectometer (Cortex Technology, Hadsund, Denmark). The MI was recorded from both inner arms and the mean of the two readings was used in the analyses.

Statistical analysis

P values for SNPs in the *NNT* region were obtained from the published CANDELA summary statistics.

C. The East & South African cohort

The summary statistics were obtained from a previous study of pigmentation evolution in Africans (Crawford et al., 2017). Details of the cohort and analyses are in the published study, so only the cohort population and phenotyping are summarized here.

Population

A total of 1,570 ethnically and genetically diverse Africans living in Ethiopia, Tanzania, and Botswana were sampled in this cohort.

Phenotyping

A DSM II ColorMeter was used to quantify reflectance from the inner underarm. Reflectance values were converted to a standard melanin index score.

Statistical analysis

P values for SNPs in the *NNT* region were obtained from the published summary statistics.

D. The UK Biobank cohort

There have been many published studies on pigmentation phenotypes in the UK Biobank (Jiang et al., 2019) and the summary statistics are publicly available at <https://cnsgenomics.com/software/gcta/#DataResource>. Details of the cohort and analyses are in the published study, so only the cohort population and phenotyping are summarized here.

Population

The UK Biobank includes more than 500,000 individuals from across the UK, with predominantly White British ancestry.

Phenotyping

Self-reported categorical questions were used to record data on skin color and ease of skin tanning.

For skin color, 6 categories were used: very fair, fair, light olive, dark olive, brown, and black (<https://biobank.ctsu.ox.ac.uk/crystal/field.cgi?id=1717>). 450,264 responses were available.

For ease of skin tanning (<https://biobank.ctsu.ox.ac.uk/crystal/field.cgi?id=1727>), participants were asked “What would happen to your skin if it was repeatedly exposed to bright sunlight without any protection”? Four categories were used: very, moderately, mildly, and never tanned. 446,744 responses were available.

For sun protection use (<https://biobank.ctsu.ox.ac.uk/crystal/field.cgi?id=2267>), participants were asked “Do you wear sun protection (e.g., sunscreen lotion, hat) when you spend time outdoors in the summer”? Four categories were used: never/rarely, sometimes, most of the time, and always. 452,925 responses were available.

Statistical analysis

P values for SNPs in the *NNT* region were obtained from the published UK Biobank summary statistics.

Meta-analysis of the cohorts

Considering the huge variation in sample size among the 4 cohorts, Fisher's method (Won et al., 2009) of combining p values from independent studies was used, in which p values for one marker across different cohorts were combined to provide an aggregate p value for the meta-analysis of that marker.

Multiple testing adjustment

Since we tested 332 independent associations, we corrected the significance threshold for multiple testing. We used the false discovery rate (FDR) method of controlling the multiple testing error rate, following the Benjamini-Hochberg procedure (Benjamini and Cohen, 2017). Applying the FDR procedure on the set of p values to achieve an overall false positive level of 5%, the adjusted significance threshold was $p = 1.01E-3$. As there is substantial LD (linkage disequilibrium) between the SNPs, a Bonferroni correction would have been overly conservative.

GWAS conditional on known pigmentation variants

MC1R is a major determinant of pigmentation, with known genetic variants associated with lighter skin color, red hair, and freckles in European populations (Quillen et al., 2019). Among the two European cohorts used in this study, individual-level data were only available for the Rotterdam Study, so the conditional GWAS analysis was conducted only in this cohort.

We retrieved the dose allele of major *MC1R* variants data from the Rotterdam studies and used them as covariates in the earlier used multiple linear regression model, in addition to the previously mentioned covariates. The association P value of the *NNT* variant is thus conditioned on the known pigmentation variants in this analysis. These conditioned P values were then compared to the original (unconditioned) P values with a Wilcoxon rank-sum test to assess whether they have been significantly altered due to the conditioning on the known pigmentation variants.

Jacobs et al., 2015 examined three functional variants in *MC1R* for their relationship with pigmentation in the Rotterdam Study: rs1805007, rs1805008, rs1805009 (Jacobs et al., 2015). Therefore, the first conditional analysis was performed using these three *MC1R* variants.

Subsequently, an additional set of well-established genetic variants in other pigmentation genes (Adhikari et al., 2019) were also used for conditioning: rs28777 (*SLC45A2*), rs12203592 (*IRF4*), rs1042602 (*TYR*), rs1800404 (*OCA2*), rs12913832 (*HERC2*), rs1426654 (*SLC24A5*), and rs885479 (*MC1R*).

Correlation between trait effect sizes and eQTL expression data

eQTL expression data corresponding to expression levels of the *NNT* transcript were downloaded from the GTEx database. For each genetic variant in the *NNT* region, we obtained the normalized effect size (NES) and P value for the alternative (non-reference) allele in each of the two skin tissues: "Skin - Not Sun Exposed (Suprapubic)" and "Skin - Sun Exposed (Lower leg)."

Correlation values were calculated between the regression coefficients for the alternative alleles of each variant from the UK Biobank for each of the three traits and the NES values corresponding to the same alleles (to ensure consistency of effect direction) in each of the two skin tissues.

QUANTIFICATION AND STATISTICAL ANALYSIS

ImageJ v1.8.0 (<https://imagej.nih.gov/ij/>) was used to quantify the immunoblots. FIJI software enabling pixel-based color quantification was used for Zebrafish analysis.

Statistical analysis

Statistical analyses were performed using GraphPad Prism 8. In general, for comparisons of two groups, significance was determined by two-tailed, unpaired Student's t tests, correcting for multiple t tests with the same two groups using the Holm-Šidák method. One-way and two-way ANOVA tests were used for comparisons of more than two groups involving effects of one or two factors, respectively, using the recommended post-tests for selected pairwise comparisons. The specific statistical tests used for experiments are described in the figure legends. P values less than 0.05 were considered statistically significant. Levels of significance are indicated by * $p < 0.05$, ** $p < 0.01$, *** $p < 0.001$, **** $p < 0.0001$; ns, not significant.

Supplemental figures

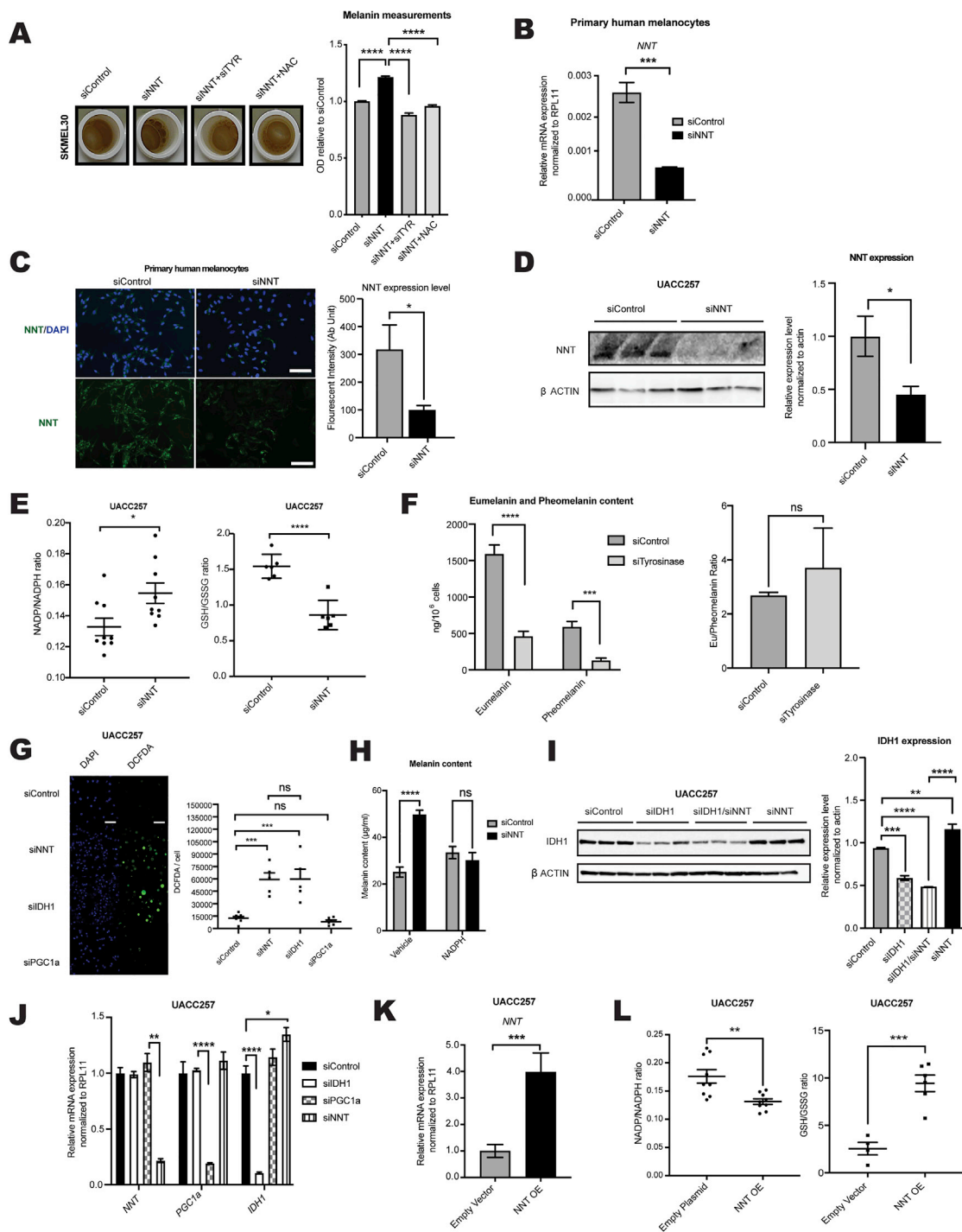


Figure S1. Inhibition of NNT increases pigmentation via a redox-dependent mechanism, related to Figure 1

(A) siNNT-induced increased pigmentation in human SK-MEL-30 melanoma cells is dependent on tyrosinase and reactive oxygen species. Left panel: Representative lysates from SK-MEL-30 cells following treatment with siControl, siNNT, siNNT + siTyrosinase (siTYR), or siNNT + 5mM NAC. Right panel: Quantification of intracellular melanin content in SK-MEL-30 cells; n = 3, analyzed by ordinary one-way ANOVA with Dunnett's post-test. (B, C) qRT-PCR analysis of *NNT* (B) and immunofluorescence of NNT (C) in primary human melanocytes treated with siControl or siNNT for 96 hours. IF staining of human NNT (Green) and nuclei (DAPI, (legend continued on next page)

blue) are shown. Scale bar 50 μ M. Relative *NNT* mRNA levels and fluorescent intensities ($n = 3$) were analyzed by unpaired, two-sided t tests. (D) Immunoblot analysis of *NNT* expression in UACC257 human melanoma cells. Band intensities were quantified by ImageJ, normalized to β -actin and plotted relative to si-Control; $n = 3$, analyzed by unpaired, two-sided t test. (E) Treatment of UACC257 cells with siNNT for 24 hours resulted in increased NADPH/NADP (Left panel, $n = 9$) and decreased GSH/GSSG (Right panel, $n = 6$) ratios. The data were analyzed by multiple t tests with the Holm-Šidák post-test. (F) UACC257 melanoma cells were treated with siControl or siTyrosinase for 5 days and eumelanin and pheomelanin were measured using HPLC techniques ($n = 3$). Absolute pigment levels (Left graph) were analyzed by ordinary two-way ANOVA, separately for eumelanin and pheomelanin. The eumelanin/pheomelanin ratio (Right graph) was analyzed by unpaired Student t test (G). Increased ROS in UACC257 cells following 48 hours of siNNT or siIDH1 treatment, but not after 48 hours of siPGCa treatment. IF images of ROS indicator DCFDA (Green) and nuclei (DAPI, blue), representative of five experiments, are displayed. Quantified results were normalized to the total number of cells and analyzed by ordinary one-way ANOVA with Šidák's post-test. (H) Increase of melanin content by siNNT is blocked by cotreatment with NADPH. Intracellular melanin content was quantified in UACC257 cells treated with siControl or siNNT for 72 hours, with 0.1 M NADPH or Vehicle (Tris-HCl, pH 8.0) added after the first 24 hours. $n = 3$, analyzed by ordinary two-way ANOVA with Šidák's post-test. (I) Immunoblot analysis of IDH1 in UACC257 cells treated with siControl, siNNT, siIDH1, or siNNT + siIDH1 together for 72 hours. Band intensities were quantified by ImageJ, normalized to β -actin ($n = 3$), and analyzed by ordinary one-way ANOVA with Dunnett's post-test. (J) qRT-PCR analysis of *NNT*, *IDH1*, and *PGC1 α* mRNAs in UACC257 cells treated with siRNA for one of those genes or siControl. qRT-PCR data are normalized to *RPL11* RNA and RNA levels are presented as fold change relative to siControl; ($n = 3$), analyzed by ordinary one-way ANOVA with Dunnett's post-test, followed by the Bonferroni correction for three ANOVA analyses. (K, L) Overexpression of *NNT* in the UACC257 cell line: (K) qRT-PCR analysis of *NNT* mRNA five days post transfection; $n = 3$, analyzed by unpaired, two-sided t test. (L) Overexpression of *NNT* resulted in decreased NADPH/NADP (Left panel, $n = 8$) and increased GSH/GSSG (Right panel, $n = 4-6$) ratios, analyzed by multiple t tests with the Holm-Šidák post-test.

All data are expressed as mean \pm SEM; * $p < 0.05$, ** $p < 0.01$, *** $p < 0.001$, **** $p < 0.0001$.

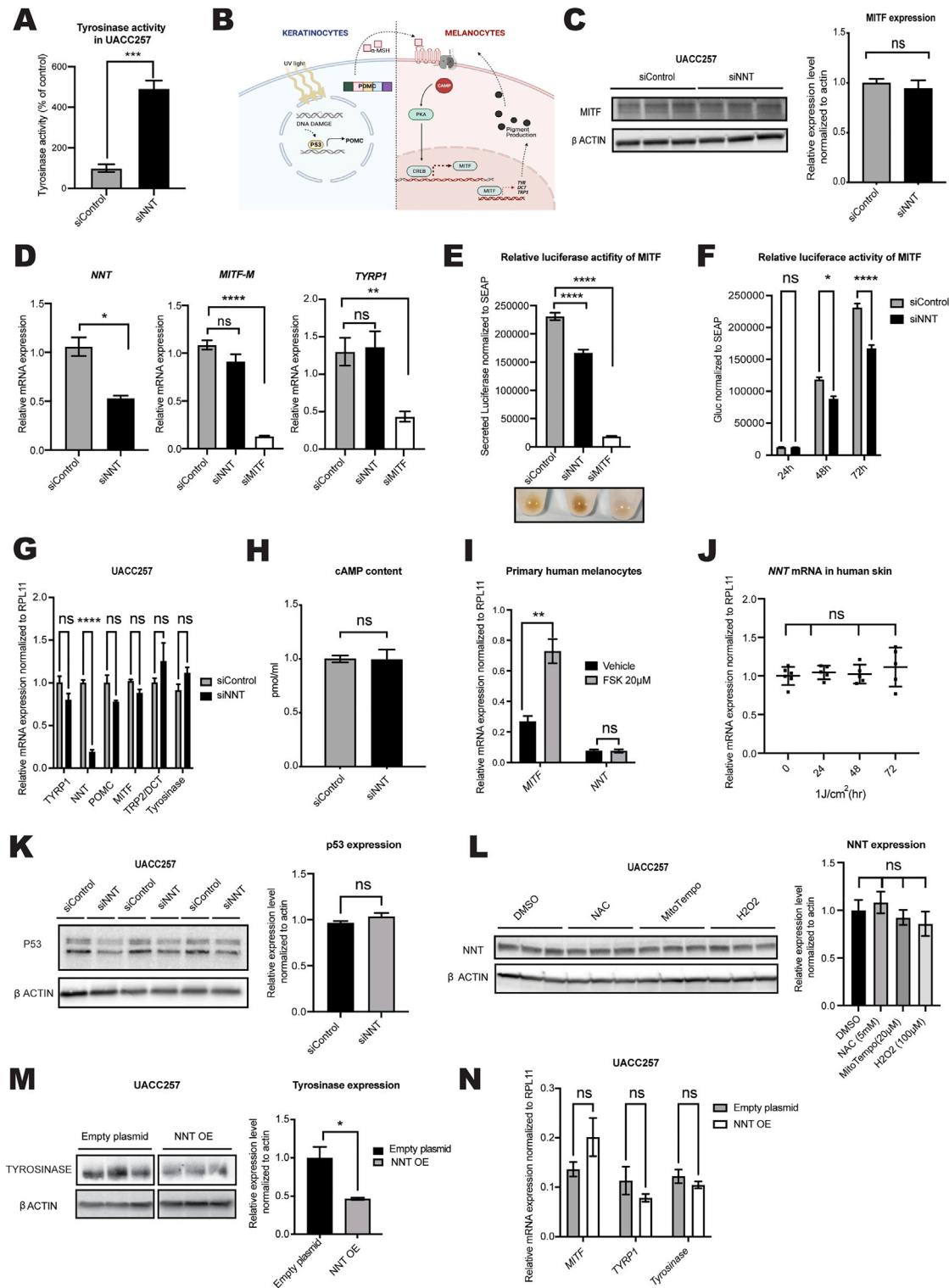


Figure S2. NNT does not affect TYR mRNA expression levels and acts independent of the cAMP pathway, related to Figure 2

(A) Tyrosinase activity increase following siNNT in UACC257 melanoma cells; n = 4, analyzed by unpaired, two-sided t test (B) Diagram of the "Tanning Pathway." Briefly, UV exposure results in DNA damage and activation of P53 in keratinocytes. *POMC* is transcriptionally activated by P53 and the pro-protein is cleaved to α -MSH, which is secreted from the keratinocyte. α -MSH binds to MC1R in the melanocyte membrane, resulting in an increase in cAMP and activation of PKA. Active PKA results in an increase of MITF, activated transcriptionally by CREB. MITF transcriptionally regulates pigmentation enzymes such as TYRP1, TRP2 and

(legend continued on next page)

tyrosinase. (C) Immunoblot analysis of MITF in UACC257 cells transfected with siNNT or siControl for 72 h. Band intensities were quantified by ImageJ, normalized to β -actin, plotted relative to siControl values ($n = 3$), and analyzed by unpaired, two-sided t test. (D-F) Analyses of UACC257 cells stably expressing secreted luciferase under the TRPM1 promoter and SEAP under the CMV promoter. The cells were treated with either siControl, siNNT, or siMITF ($n = 3$): (D) qRT-PCR analysis of *NNT*, *mMITF* and *TYRP1* 72 hours post siRNA transfection. Data were normalized to *RPL11* RNA, analyzed by unpaired, two-sided t test (*NNT*) or ordinary one-way ANOVA with Dunnett's post-test (*mMITF* and *TYRP1*). (E) Luciferase secretion normalized to secreted SEAP 72 hours post siRNA transfection, showing decreased luciferase activity following siMITF and siNNT, analyzed by ordinary one-way ANOVA with Dunnett's post-test; representative cell pellets (1×10^6 cells) are below the graph. (F) Luciferase secretion normalized to secreted SEAP 24, 48 and 72 hours post siRNA transfection was analyzed by repeated-measures two-way ANOVA with Sidak's post-test. (G) qRT-PCR analysis of *NNT*, *MITF*, *TYRP1*, *TRP2/DCT*, *NNT*, *tyrosinase*, and *POMC* in UACC257 cells 72 hours post transfection of siNNT or siControl. Data were normalized to *RPL11* RNA, presented as fold change relative to siControl ($n = 3$), and analyzed by multiple t tests with the Holm-Sidak post-test. (H) cAMP content of UACC257 cells transfected with siNNT or siControl for 48 h, measured by cAMP ELISA and normalized to siControl cells; $n = 3$, analyzed by unpaired, two-sided t test. (I) Primary human melanocytes were starved for 24 hours and Forskolin (FSK; $20 \mu\text{M}$) was added to the medium for 2 hours. qRT-PCR analysis of *NNT* was performed with *MITF* as a positive control for the treatment. The data were normalized to *RPL11* RNA ($n = 3$) and analyzed by multiple t tests with the Holm-Sidak post-test. (J) No change in *NNT* mRNA upon UVB. Abdominal skin was irradiated with $1\text{J}/\text{cm}^2$ UVB, skin was collected at 0, 24, 48 and 72 hours post UVB, and qRT-PCR analysis of *NNT* was performed. The data were normalized to *RPL11* RNA and presented as fold change relative to $t = 0$. $n = 5-6$ (two different donors), analyzed by ordinary one-way ANOVA with Dunnett's post-test. (K) Immunoblots of P53 and β -actin in UACC257 cells following siControl or siNNT treatment for 72 hours. (L) Immunoblot of *NNT* and β -actin in UACC257 melanoma cells (Left panel), daily treatment with NAC (5 mM), MitoTEMPO ($20 \mu\text{M}$) and H_2O_2 ($100 \mu\text{M}$) for 72 hours ($n = 3$) analyzed by ordinary one-way ANOVA with Tukey post-test. (M) Immunoblots of tyrosinase and β -actin in UACC257 melanoma cells (Left panel), showing decreased tyrosinase protein levels following overexpression of *NNT* for 12 days. Band intensities were quantified by ImageJ, normalized to β -actin and plotted relative to siControl values (Right Panel). ($n = 3$), analyzed by unpaired, two-sided t test. (N) qRT-PCR analysis of *MITF*, *TYRP1* and *tyrosinase* mRNAs in UACC257 cells that overexpressed *NNT* (*NNT* OE), compared to control (Empty Vector). The data were normalized to *RPL11* RNA ($n = 3$) and analyzed by ordinary one-way ANOVA with Dunnett's post-test, followed by the Bonferroni correction for three ANOVA analyses.

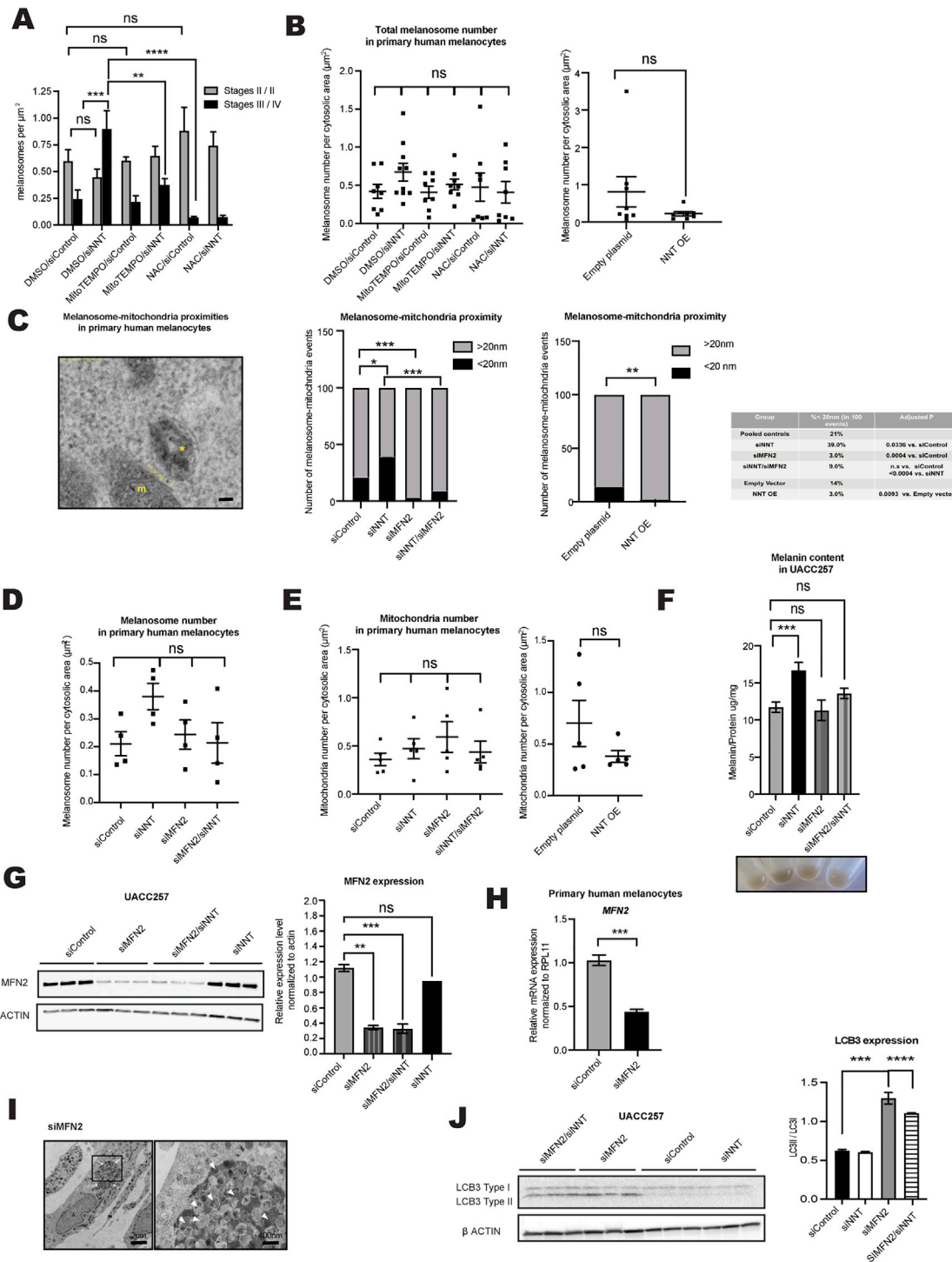


Figure S3. NNT knockdown enhances melanosome maturation, melanosome-mitochondria proximity, and pigmentation by NNT knockdown, related to Figure 2

(A) Enhanced melanosome maturation induced by siNNT in human primary melanocyte cells is blocked by NAC (5 mM) or MitoTEMPO (20 μ M) (daily treatment for 96 h). The number of melanosomes per μ m² in the classified stages is represented. $n = 4-5$ cells, analyzed by ordinary two-way ANOVA with Sidák's post-test (B) The total number of melanosomes per μ m² in primary human melanocytes is not altered by siNNT and/or daily treatment with NAC (5 mM) or MitoTEMPO (20 μ M) for 96 hours (Left graph, $n = 8-10$, analyzed by ordinary one-way ANOVA with Dunnett's post-test) or by overexpression of NNT (Middle graph, $n = 8-10$), analyzed by unpaired, two-sided t test. The total numbers of mitochondria per μ m² by overexpression of NNT (Right graph, $n = 5$) is not altered. (C) Measurements of proximities between melanosomes and mitochondria were quantified in FIJI (ImageJ) by applying a customized macro to TEM micrographs ($n = 100$ events per

(legend continued on next page)

condition). Melanosome-mitochondria proximities closer than 20 nm are considered melanosome-mitochondria close appositions/contacts. Right panel: FIJI graphical user interface showing a TEM micrograph of mitochondria (m) and a melanosome (*) with a yellow line indicating the Euclidean distance between melanosome and mitochondrion surfaces, quantified with a customized macro to measure distances between two surfaces. Scale bar 400 nm. Table shows the percentages and, in parentheses, the fractions of melanosome-mitochondria proximities that were < 20 nm. Denominators are the total number of measurements (events) performed in each group. Adjusted P values were determined by pairwise F-tests of the control group to each of the other groups, followed by the Bonferroni correction for three comparisons. (D-E) The total numbers of melanosomes (D) and mitochondria (E) per μm^2 in primary human melanocytes is not altered; $n = 5$ cells, analyzed by ordinary two-way ANOVA with Sidák's post-test. (F) MFN2 enables siNNT-mediated pigmentation. Top panel: Quantification by spectrophotometry of intracellular melanin content of UACC257 human melanoma cells treated with siControl, siNNT, siMFN2 + siNNT, or siMFN2 for 72 hours. $n = 3$, analyzed by ordinary one-way ANOVA with Dunnett's post-test. Bottom panel: Representative cell pellets (10^6 cells). (G) Immunoblot analysis of MFN2 expression in UACC257 human melanoma cell lines. Band intensities ($n = 3$) were quantified by ImageJ, normalized to β -actin, and analyzed by ordinary one-way ANOVA with Dunnett's post-test. (H) qRT-PCR analysis of *MFN2* in primary human melanocytes that were transfected with siMFN2. The data were normalized to *RPL11* RNA, plotted relative to the control ($n = 3$), and analyzed by unpaired, two-sided t tests (I) siMFN2 resulted in accumulation of large autophagosomes (white arrows), containing numerous melanosomes (arrowheads), in normal human melanocytes. Scale bar 2 μm . (J) Immunoblot analysis of LC3B in UACC257 cells treated with siMFN2, siNNT, siMFN2+siNNT, or siControl for 72 hours. Band intensities were quantified by ImageJ and normalized to β -actin. The ratios of LC3BII to LC3BI were plotted ($n = 3$) and analyzed by ordinary one-way ANOVA with Dunnett's post-test. All data are expressed as mean \pm SEM; * $p < 0.05$, ** $p < 0.01$, *** $p < 0.001$, **** $p < 0.0001$.

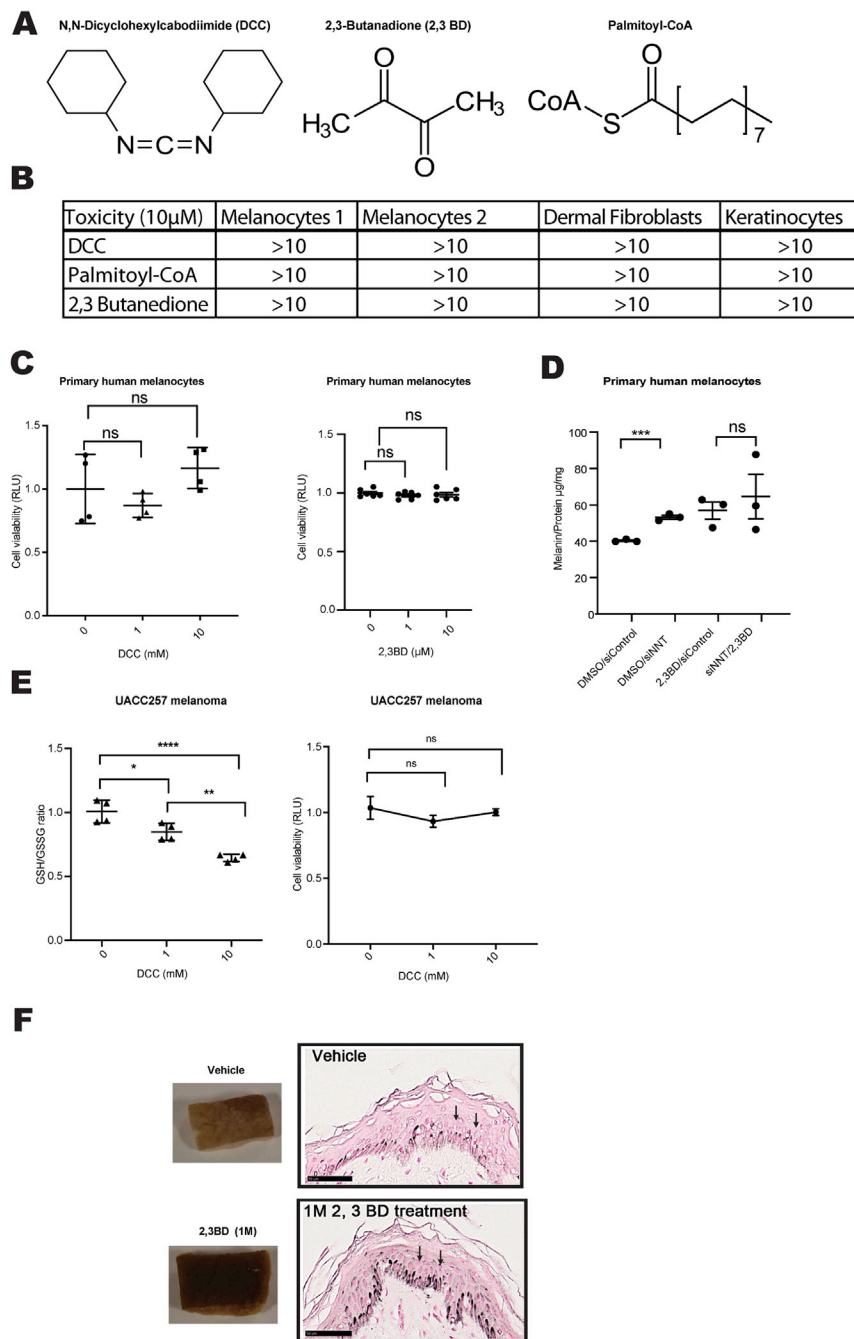


Figure S4. NNT inhibitors are non-toxic *in vitro*, related to Figure 3

(A) Chemical formulas of all three published NNT inhibitors. (B) Viability measurements showed no significant toxicity after treatment of human melanocytes, dermal fibroblasts, and keratinocytes with up to 10 μ M of DCC, Palmitoyl-CoA, or 2,3BD. (C) Treatments with different doses of DCC (Left graph) or 2,3 BD (Right graph) had no impacts on cell viability. The data were plotted relative to vehicle treatment (0) and analyzed by ordinary one-way ANOVA with Dunnett's post-test ($n = 4$). (D) Intracellular melanin content normalized to total protein levels in primary human melanocytes that were treated with siControl or siNNT for 24 hours, followed by incubation with 2,3 BD (2 mM) or DMSO vehicle for 72 hours. $n = 3$, analyzed by ordinary one-way ANOVA with Šidák's post-test. (E) Treatments with different doses of DCC had no impact on cell viability (Right graph), but resulted in decreased GSH/GSSG ratios (Left graph) in the UACC257 human melanoma cell line. $n = 4$, analyzed by ordinary one-way ANOVA with Tukey's (Left graph) or Šidák's (Right graph) post-test. (F) Fontana-Masson staining of melanin in human abdominal skin 5 days after a single treatment of 2,3BD (1M), showing supranuclear capping (Black arrows) in keratinocytes of 2,3BD-treated skin. Scale bar 50 μ M

All data are expressed as mean \pm SEM; * $p < 0.05$, ** $p < 0.01$, **** $p < 0.0001$.

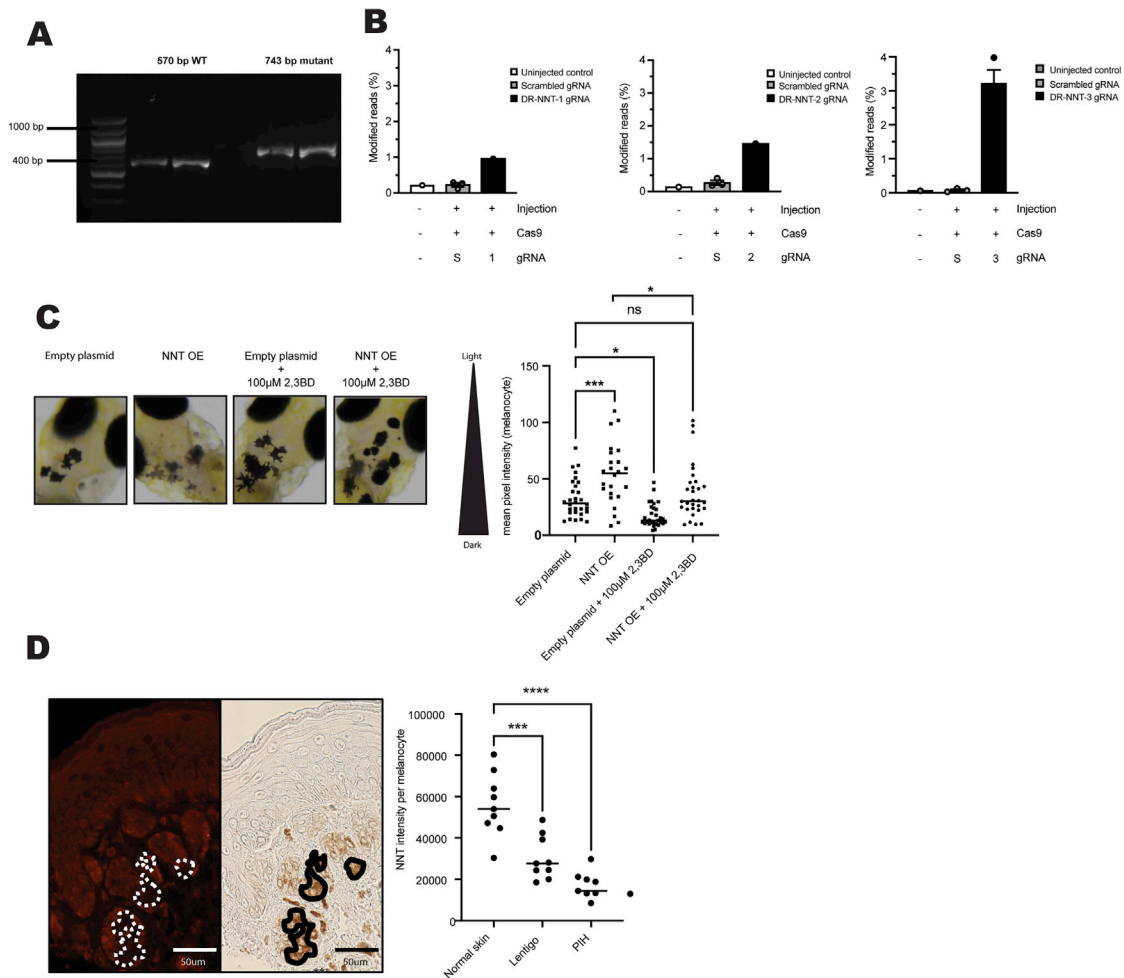


Figure S5. NNT regulates pigmentation in mice, zebrafish, and human pigmentation disorders, related to Figure 4

(A) Agarose gel showing PCR genotyping of DNA from C57BL/6J mice (single 743 bp product indicates homozygous 5-exon deletion in the *Nnt* gene) and C57BL/6NJ mice (single 570 bp product indicates homozygous wild-type *Nnt* gene). (B) Modification of NNT sites in zebrafish using WT SpCas9. Editing was assessed by next-generation targeted amplicon sequencing. (C) Zebrafish overexpressing NNT (NNT OE) or empty plasmid were treated at 3 days post fertilization with 100 µM of 2,3BD or vehicle for 24 hours. A representative image has been displayed. Results of mean melanocytic brightness, quantified by pixel-based analysis are shown in the graph at right; Empty plasmid (n = 12 fish; 30 melanocytes), NNT OE (n = 10 fish; 24 melanocytes), Empty plasmid + 2,3 BD (n = 8 fish; 30 melanocytes), NNT OE + 2,3BD (n = 11 fish; 31 melanocytes), analyzed by ordinary one-way ANOVA with Dunnett's post-test (D) Representative images of the specific areas of hyperpigmentation in human lentigo-affected skin after staining for NNT (left image, red) or Fontana Masson (right image). Graph at right shows NNT signal intensities in melanocytes of healthy and lesional skin. n = 9 (bars indicate means), analyzed by ordinary one-way ANOVA with Dunnett's post-test.